2020

Production and Elastomer Compatibility of Renewable Fuels

Alan Felix
University of Central Florida

PRODUCTION AND ELASTOMER COMPATIBILITY OF RENEWABLE FUELS

by

ALAN FELIX
B.S. University of Central Florida, 2018

A thesis submitted in partial fulfillment of the requirements
for the degree of Master of Science in Mechanical Engineering
in the Department of Mechanical and Aerospace Engineering
in the College of Engineering and Computer Science
at the University of Central Florida
Orlando, Florida

Fall Term
2020

ABSTRACT

Hydrocarbon fuel plays an essential role in modern day society and significant research effort is put forth for fuel characterization, performance optimization, and new procedures for synthesis. Despite the eventual and inevitable shift away from hydrocarbon fossil fuels to more renewable energies, investigations into liquid hydrocarbons remain useful while governments slowly adopt and integrate alternative energies.

Many hydrocarbon fuel alternatives can potentially bridge the gap between today's heavy reliance on fossil fuels and future complete adaptation of clean energy. One such alternative is biofuel, which is still hydrocarbon based but is made from bio-materials, most notably plants. Widespread use of biofuels for everyday transportation would increase demand, requiring increased planting of biomass sources which would act to remove CO_2 from the atmosphere. A small, but not insignificant improvement to our current practices. A second alternative is the synthesis of fuel from low value chemical feedstock, and even waste products. This option provides the added benefit of potential removal of harmful chemicals from waste streams and producing valuable chemicals from them.

This thesis will focus on aspects of these two fossil fuel alternatives: properties of biofuels and hydrocarbon synthesis from syngas. In the first, biofuel-elastomer interactions are investigated to evaluate the compatibility of new biofuels in existing engine systems. It is commonly known that elastomer seals, used for leak prevention in fuel lines, undergo structural changes when exposed to hydrocarbon fuel. We have shown here that these same effects are present for biofuel compounds to differing degrees. Studies were performed in the short- and long-term using ASTM

procedure to determine the extent of structural change and degradation as well as the time scale on which it occurs.

The focus of the second study is the synthesis of higher order alcohols from chemical feedstocks such as syngas (a mixture of hydrogen and carbon monoxide). It has been observed that methanol is produced by flowing syngas over copper catalysts. However, the carbonylation of methanol to form longer carbon chains has therefore not been well characterized. Thus, the products of methanol and carbon monoxide flow over silica-supported Au-MoS_2 were studied experimentally to find production of acetaldehyde. A likely chemical pathway to acetaldehyde formation was determined using density functional theory (DFT) modelling.

This is dedicated to my mother and father, sister and cousins, my son and love of my life fiancee, closest of friends and loved ones for never giving up on me and always giving me support. You all are the reason why I fought as hard as I did to achieve this goal so thank you for being my motivation and inspiring me to be the best engineer I can be. Although I had ups and downs throughout this journey you all were proud of me from start to finish.

Also, to my grandmother who passed away a few years ago and never got to see her grandson graduate, I love you and I know you have been watching over me this entire time. I love you all and am beyond grateful to have you all in my life.

ACKNOWLEDGMENTS

First and foremost I would like to acknowledge my research adviser, Dr. Richard Blair. I would like to deeply express my gratitude to him for giving me my first research position, allowing me to work in his lab as an undergrad despite having little prior exposure to chemistry. Dr. Blair taught me very early on during the (EK laboratories days) fundamentals of science and general procedures within a research environment. As an undergraduate, Dr. Blair assigned me a heavily chemistry-focused project under the supervision of Deepti Siddhanti, which I grew to enjoy very much and led me to appreciate interdisciplinary projects. Dr. Blair encouraged me to pursue a masters degree in engineering, which I would not have sought without his help and mentorship. I appreciate the work and sacrifices he made for me to get this degree and for helping me gain the confidence I needed in my knowledge of the many aspects of science.

I would like to thank my graduate faculty adviser, Dr. Jayanta Kapat, for his academic support over the last two years. Thank you for fighting for me and not giving up when we faced numerous challenges with certain departments on campus. I am grateful for everything you've done for me and your much needed support. I consider this to be a significant factor in the eventual completion of my degree.

I would like to thank the last member that served on my committee: Dr. Subith Vasu. You all showed patience and worked great with me. I would also like to thank Dr. Raman and all of her students for their help in a collaborative project which required instruments and analysis work.

I would like to give a shout out to the many lab friends and fellow students that have extended their hand and been a significant part of my journey through graduate school. Starting with Dr. David Nash, Deepti Siddhanti, Katerina Chagoya, and Dr. Zhilin Xie. Katerina, thank you for all the assistance you have giving me all the way back to EK Laboratories. You have been a true friend and supporter, and I will cherish all of the memories created with you and everyone in the Blair lab group.

TABLE OF CONTENTS

LIST OF FIGURES

LIST OF TABLES

CHAPTER 1: INTRODUCTION AND LITERATURE REVIEW

1.1 Biofuels

Currently, the world's primary source of energy is derived from fossil fuels. Approximately 63% of today's usable electrical energy comes from fossil fuels, 20% from nuclear energy, and 18% from renewable energy sources[1]. Fossil fuels, which provide natural gas, coal, and petroleum, are the primary source of greenhouse gas emissions and are destructive to our climate. At the current rate of carbon dioxide emissions from fossil fuels, roughly 12-15 years remain of the carbon budget[2]. The carbon budget is the quantity of human-emitted carbon dioxide that can be released without exceeding a global temperature rise between 1.5°C and 2.0°C.

Renewed focus on biofuels arises also from the knowledge that fossil fuel reserves are declining, and continued reliance will not be sustainable in the future. Biofuels have a major advantage in today's current market. They provide employment opportunities in rural areas where biomass can be grown in large quantities, and also throughout the production process. The steady increase in crude oil prices has caused many companies to prefer biofuels for the decreased cost, since most biofuels can be derived from wheat, corn, soybean, or sugarcane.

1.2 The Problem of Seal Swell

The function of elastomer seals within engine systems is to prevent leakage of fuel. This is accomplished by implementing o-rings or other seals to create positive pressure against joined surfaces, thereby preventing any form of leakage. These seals are implemented within cars, jets, and other engines for this purpose. Seal failure can be catastrophic, can potentially lead to injury or death, and is very expensive to repair in the event of a failure. An infamous instance of such a failure occurred on January 28th, 1986 when the Space Shuttle Challenger exploded midair. It was

later determined that the critical factor of this incident was the result of cold weather cooling essential elastomers below their glass transition temperature prior to the launch.[3] O-rings do not perform well under reduced temperature, which cause them to lose flexibility and become brittle.

The compositional makeup of most elastomer seals involve random arrangements of long-chain molecules coupled via crosslinks[4]. The spaces between chains are occupied by chemical fillers and plasticizers to produce the overall structure and elasticity, and to decrease cost. The incompatibilities of the fuel and these sealing materials can lead to swelling or shrinking, and significant changes in mass, hardness, and elasticity. O-ring degradation such as tears, nicks and gashes were seen in the long term gasoline and diesel experiments. This strongly suggests that failure of the seal can quickly lead to failure of other components in an engine. Although chemical-elastomer compatibility are generally available on the manufacturer's website, that information is not specific enough to be useful to gain knowledge on *in situ* longevity of the o-ring. Also to note that the information giving by the manufacture will only include classes of molecules and not the specific fuel you want to use.

1.3 Higher Order Alcohol Formation

The study of the mechanism of catalytic conversion of methanol into mixed alcohol blends over molybdenum disulfide catalysts was investigated. MoS_2 is known to be an efficient catalysis for the conversion of syngas to methanol, however the mechanism of obtaining higher order alcohols is not as well known. Syngas or synthesis gas is a mixture composed of hydrogen and carbon monoxide. The start of this product goes back as early as the 20^{th} century and has been used to produce mixtures of methanol and higher alcohols. In this report, a focus on carbonylation of

methanol as the most fundamental C-C coupling step was looked into. It was found that acetaldehyde is an intermediate product formed prior to methanol realization.

CHAPTER 2: TOWARDS HIGHER ALCOHOL FORMATION USING A SINGLE-LAYER MoS_2 ACTIVATED Au ON SILICA: METHANOL CARBONYLATION TO ACETALDEHYDE

2.1 Introduction

The formation of higher alcohols from syngas is an important goal in the quest for economic and sustainable transformation of biomass into transportation fuels[5]. A necessary step for its realization is efficient C-C coupling involving oxygenate small molecules such as carbon monoxide and methanol[6, 7]. Important work by Haruta *et al* showed that CO oxidation is catalysed by supported nanoscale gold particles[8]. This revealed that the catalytic activity of metals that are relatively inert in the bulk can be enhanced through nanostructuring[9]. In recent work,[10, 11] it has been shown that single-layer molybdenum disulphide (MoS_2) coating can transform an otherwise inert substrate, silica, into a catalytic active surface for CO oxidation by gold nanoclusters. This is similar to results obtained on reducible oxides, such as titania and ceria[12-18]. Concomitant computational efforts have predicted a number of feasible, low-barrier reaction pathways on thus supported gold nanoparticles,[10, 19] in contrast to the catalytically largely-inactive surface of bulk gold, of gold on pristine silica, or on other 2D materials like graphene[20-22]. Here, we address the carbonylation of methanol as the most fundamental C-C coupling step that can ultimately lead to higher alcohol formation from a lower alcohol. The mixture of methanol and carbon monoxide was investigated as an approximation of the reaction stream from syngas over the catalysts surface; hydrogen, water and other species were excluded to maintain a system simple enough to model computationally. Syngas may be obtained from biomass gasification, and conversion to higher alcohols is a potential rapid pathway toward sustainable and renewable fuels.

Molybdenum disulphide has been investigated for a wide range of catalytic applications. MoS_2 with cobalt and alkali modifiers is the key catalyst material in industrial hydrodesulphurization; notably, the industrial catalyst material resembles a few-layer film of supported MoS_2[23]. Alkali modification of this material has also been proposed for alcohol formation[24-32]. The mechanistic aspects of these studies have been focused on the hydrogenation step, in particular the initial CO hydrogenation to produce methanol. To further the understanding of catalysis over this material, our study focuses on the extension of the carbon chain toward higher alcohols through the carbonylation of methanol.

MoS_2 has gained prominence as a catalyst for hydrogen evolution;[33, 34] its activity has been attributed to edge sites based on low-temperature measurements,[35] and related materials that feature large number of exposed edge sites have been prepared and validated in some catalytic applications[36-42]. We sought to investigate the interaction between the support and catalytically active nano-clusters. By producing polycrystalline continuous single-layer MoS_2 coatings over several centimetre in diameter,[43] we avoid the activity of edge sites and can focus solely on grain boundaries and metal-MoS_2 sites. This simplified structure allows us to probe the fundamental chemistry of chain lengthening. Dr. Ludwig Bartels was in charge of producing the polycrystalline single-layer of MoS_2 coated over a fused silica window with gold nanoparticles depositioned on the surface of the MoS_2.

Surprisingly, the carbonylation of methanol was catalysed over the Au-MoS_2 structures to yield acetaldehyde. Using a laminar flow reactor, acetaldehyde formation occurred at fairly low temperatures (as low as 393 K), on single layer MoS_2 films, decorated by nanoscale gold islands. Density functional theory (DFT) modelling was used to find a plausible pathway for this important carbon-carbon coupling step. DFT was done by Dr. Talat S. Rahman and her research group.

2.2 Results and Discussion

2.2.1 Theory

Accompanying density functional theory (DFT) calculations validate the feasibility of the formation of carbon-carbon bonds at the surface of MoS_2-supported Au nanoparticles from carbon monoxide and methanol alone. Continuing the success of previous computational work[44] in which the alcohol synthesis from syngas (CO and H_2) was shown to be favourable on Au_{13} nanoparticles stabilized by interactions with a single layer of MoS_2, we use the same supercell setup to study the formation of a bond between adsorbed methyl and carbonyl species to form acetyl.

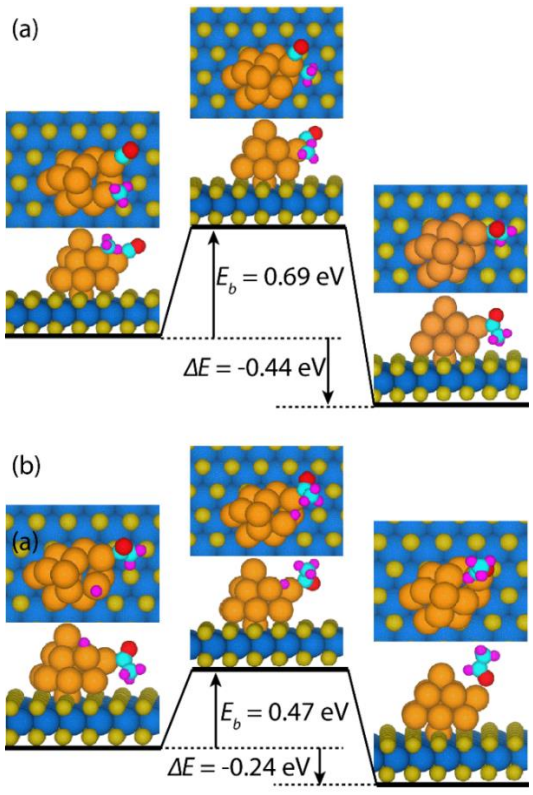

Figure 1. Reaction pathways of CH3* + CO* → CH3CO* (a) and CH3CO* + H* → CH3CHO* (b). Left, center, and right images show both top and side views of initial, transition, and final states, respectively. Blue, yellow, gold, cyan, red, and magenta balls represent Mo, S, Au, C, O, and H atoms, respectively. Eb and ΔE are activation barrier and reaction energy, respectively.

Collaborators from Dr. Rahman's group at the University of Central Florida reported that the DFT calculations are based on the plane-wave basis set and the pseudopotential method employing the generalized-gradient approximation (GGA) in the form of the Perdew-Burke-Ernzerhof (PBE) [45] functional to take into account the electron-exchange interaction together with DFT-D3 correction [46] for inclusion of van der Waals interactions. Transition states and reaction activation energy barriers are calculated using the climbing-image nudged elastic band (CI-NEB) method.[47, 48] Further details of the calculations can be found in previous work.[44] We consider the formation of acetaldehyde by studying the most likely process steps: CH_3* + CO* → CH_3CO* and CH_3CO* + H* → CH_3CHO*, where CH_3* and H* species are produced through the adsorption and dissociation of methanol on the stabilized gold surface (* designates adsorbed species). Additionally, CO is required to reduce residual O* species via O* + CO* → CO_2*, a highly exothermic reaction (ΔE = -2.23 eV) with a barrier of 0.06 eV, as also described elsewhere.[10, 11] Figure 1a,b shows the initial state, transition state, and final states of the CH_3* + CO* → CH_3CO* and CH_3CO* + H* → CH_3CHO* reactions. Our calculations indicate that the formation of a bond between the adsorbed CH_3* species and a CO* molecule on Au_{13} is energetically favorable as the reactions are exothermic and the activation barriers comparatively low: 0.69 eV for the acetyl formation (I) (Figure 1a) and 0.47 eV for the hydrogenation of acetyl to acetaldehyde (II) (Figure 1b). The resultant CH_3CHO* desorbs with a desorption energy of 0.45 eV.

Close inspection reveals that the site with the lowest pathway barriers corresponds to the least coordinated gold atom on the cluster, at which the binding of the reactants is strongest. Such sites are more prevalent on nanoscale gold clusters. This finding highlights the importance of

nanoclusters for this reaction to proceed. Single-layer of MoS_2 serves to provide a surface on which dispersal of gold into nanometer-scale clusters is favorable.[19]

2.2.2 Experiment

The samples shown below (Figure 2a) exhibit the typical Raman peak positions for single-layer MoS_2 films for E_{2g} and A_{1g} at 385.5 cm^{-1} and 404.9 cm^{-1} (separation 19 cm^{-1}).[49] Before gold deposition, the photoluminescence of the substrate material was intense and centered at 1.91 eV with a full-width at half-maximum of ~0.1 eV, the optical bandgap of single-layer MoS_2 (Figure 24).[50, 51] After gold deposition, the photoluminescence is quenched. This indicates that despite the incomplete surface coverage, there is a quenching centre within the size of practically any exciton created on the surface. This suggests efficient dispersion of gold on MoS_2/SiO_2, in contrast to gold on bare silica or graphene. Direct scanning electron microscopy (SEM) imaging of a test sample with a 30 nm silica film on silicon shows tiny, point-like gold particles near the limit of the instrument's resolving power (Figure 3). Image analysis using ImageJ [52] showed that the majority of these range from diameters of 1-5 nanometers in size, i.e. in a useful size range for catalytic activity.[53-55] The spatial homogeneity of the sample was verified by determining the Raman peak separation and photoluminescence position along a line across the substrate (Figure 2b). The Raman spectra was completed by Dr. Peter A. Dowben.

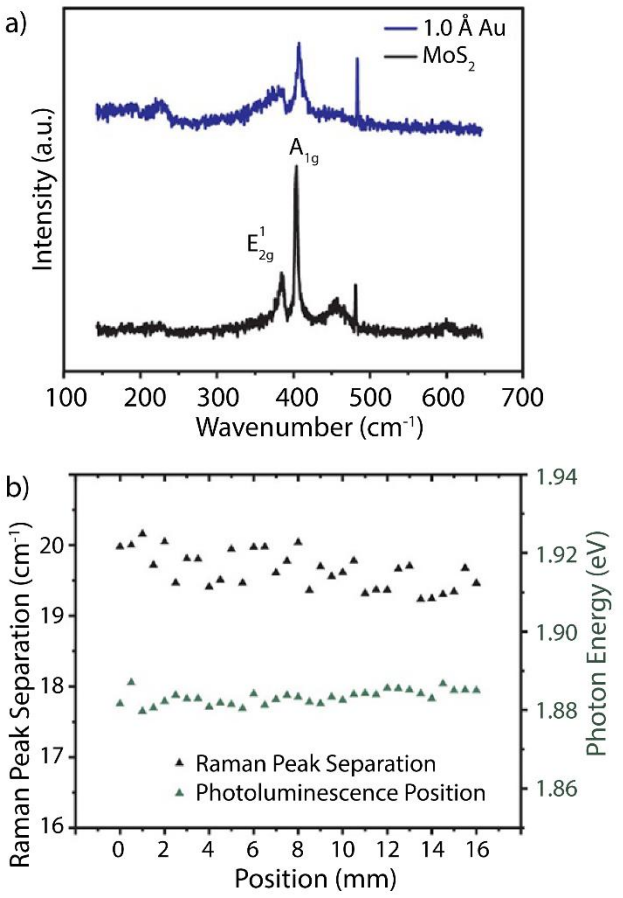

Figure 2. The Raman spectra of a single-layer MoS2 sample before (black) and after (color) sub-monolayer gold deposition (a) and homogeneity of the single-layer MoS2 film across the fused silica substrate (b).

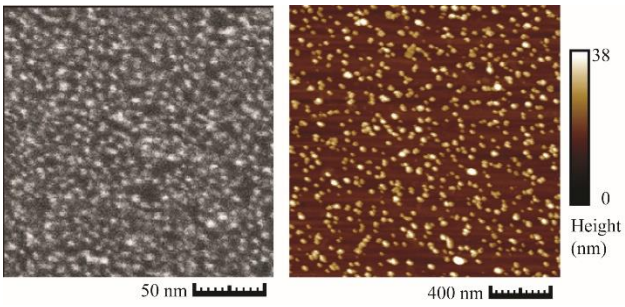

Figure 3. Initial deposition of Au, on a single layer MoS_2 film coating a 30nm silica test film, produced well-dispersed particles ranging from 1-5 nm (SEM image, left). After two cycles on stream at 150 ˚C, a similarly coated sample shows particle agglomeration producing a distribution centred around 40 nm (AFM right).

The reactant stream consisted of CO gas at 308 kPa bubbled through a methanol reservoir at 20 ˚C. At this temperature methanol has a vapour pressure of 13 kPa or 4.2% of the feed stream. Prior to the reaction, the reactor was purged with argon gas and heated to the reaction temperature of 150°C. After 120 minutes on stream a sample was taken for GC-MS analysis by a sampling port. Comparison of the product peak with GC-MS chromatogram of a standard acetaldehyde/methanol mixture (Figure 23) indicated the observed peak in the TCD chromatogram is acetaldehyde. Carbon monoxide (RT= 2.295 min), acetaldehyde (RT=3.305 min), methanol (RT=4.245 min) and water (RT=5.149 min) were detected in TCD chromatograms. Water was detected in all reactions (with and without gold) at very low concentrations.

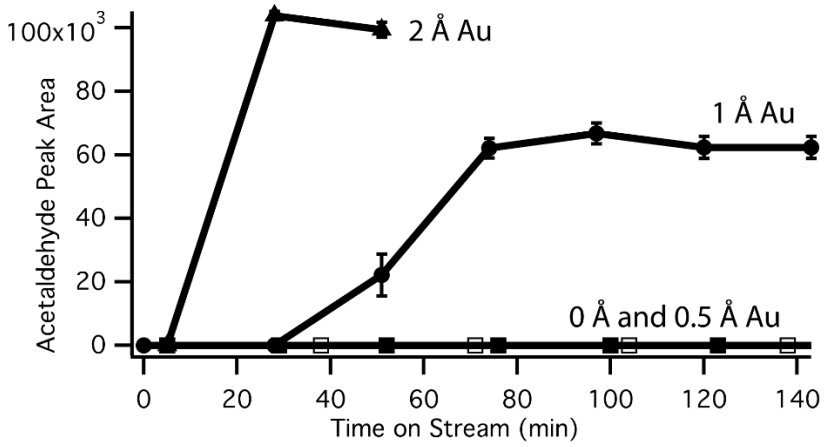

Figure 4. The integrated acetaldehyde peak intensity, as a function of the on-stream time at 150 ˚C, shows the onset of activity after a 20-30 minute induction period. Time zero is when the reactor, at temperature, was switched from an argon to reactant feed.

We investigated the stability of the catalyst by running the reactor for 140 minutes and reusing a catalyst after on stream. The 1Å catalyst was utilized for 140 minutes, stored in an Ar-filled glovebox for 20 days and reused. Catalytic acetaldehyde formation was still observed. Figure 4 shows the production of acetaldehyde as time on stream for all samples. While we observe

a slight drop initially, we find that subsequently the reaction proceeds at a consistent rate. The delay in the onset of catalysis is related to the flow rate of the reactant stream. This is the time to purge the 13.4 cm^3 transfer line volume when switching from argon purge to reactant stream. The 2Å sample had a higher reactant flow rate. A blank consisting of the MoS_2 coated substrate without gold did not produce measurable amounts of acetaldehyde.

Atomic force microscopy was used to analyse the effect of on-stream time on the gold dispersion (Figure 4b). It was found that the gold particles coalesced, and the particle size distribution was centered around 40 nm (Figures 25-28). Aggregation of gold particles is not unexpected as capped gold has been shown to behave similarly in solution experiments with temperatures over 120 ˚C[56] and platinum is predicted to have a high mobility on a MoS_2 surface.[57]

2.3 Conclusion

The deposition of gold nanoparticles on a single layer of MoS_2 on an inert fused silica substrate provides a surface suitable for the carbonylation of methanol to acetaldehyde. Results presented here showcase the catalytic promise of gold nanoparticles supported on single layers of MoS_2, discussed elsewhere, even as the mean particle size increases during usage.[5] Our DFT based calculations have proposed MoS_2 supported Au nanoparticles as suitable catalysts for the of conversion of syngas to methanol.[58] More recently we have shown the possibility of extending this reactivity to produce higher alcohols.[59] Findings here highlight an important first step towards the formation of higher alcohols from methanol or even syngas using thin layers of MoS_2 and less than a monolayer of gold. We show that a non-active support such as silica can be converted into an active support though the application of single layers of active support.

Although, MoS_2 is a commodity mineral, it is limited in occurrence. We show that a very small amount of MoS_2 is required to produce an effective catalyst. A monolayer on 2 mm beads would be an equivalent MoS_2 loading of 1.88 ppm and an Au loading of 1.15 ppm. A cubic meter of supported catalyst prepared in such a way would require 146 mg of MoS_2 and 90 mg of gold. The low reaction temperatures and pressures (308 kPa and 393 K) further support the appeal of this approach. Additionally, acetaldehyde can be oxidized to acetic acid yielding a route without the need for iodides. Although the basal plane of MoS_2 is inert edge sulfur vacancies are thought to be the key to hydrodesulfurization and hydrodenitrogenation activity over MoS_2.[60] Our results illustrate a mechanism by which the basal plane and grain boundaries can influence the chemical activity of a metal catalyst. Furthermore, our results also speak to sustained reactivity of Au nanoparticles in a scenario in which inert substrates can be first shaped into desired structures that optimize reactant and heat flow and serve as an inexpensive scaffold for a composite that bestows catalytic activity on them.

2.4 Experimental Section

A Ø1.5 cm x 1 mm thick fused silica window (Esco Optics) was homogeneously coated with a single polycrystalline layer of MoS_2 decorated by nanoscale gold islands corresponding to an average gold coverage of 0.5 Å, 1Å, and 2Å or approximately 1/6, 1/3, and 2/3 of a monolayer respectively. Figure 5b shows the preparative effort schematically and Figure 5c depicts the fused silica window after single-layer MoS_2 and gold deposition.

To make the supported catalysts, we have utilized a technique for coating inert oxides by an MoS_2 films of controlled integer layer number, as reported elsewhere.[43] The original work focused on MoS_2 films on a dry oxide SiO_2 layer on a silicon wafer substrate. The single- and few-

layer MoS_2 growth technique is based on heating molybdenum filaments to white heat (>1500 K) under high vacuum followed by exposure to carbon disulphide. Decomposition of the disulphide on the Mo filament surface results in volatile MoS_x precursors, which are precipitated onto the substrate. The substrate is held at a temperature where MoS_2 island growth and desorption is at equilibrium. Reference sample for scanning electron microscopy were prepared on a thin (30 nm) silicon dioxide film on a doped silicon substrate. Gold was deposited with an e-beam evaporator monitored by a quartz crystal microbalance. Deposition rates were calculated from the measured mass increase and converted to Ångstroms of gold per minute. Values below the atomic diameter of gold (3.2 Å) indicate incomplete (sub-monolayer) coverage.

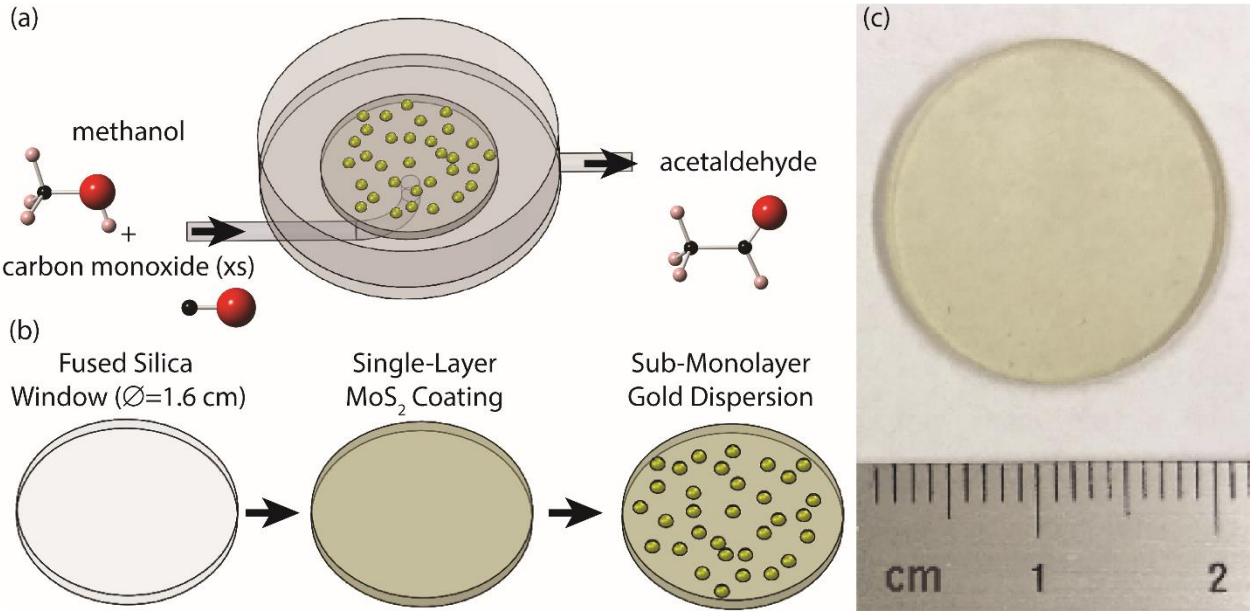

Figure 5. A schematic representation of the catalyst preparation and catalytic evaluation in a laminar flow reactor(a,b); The Ø1.5 cm fused silica window coated with a single-layer of MoS2 and deposition of gold exhibits a yellowish color (c).

Reactor studies were performed in a laminar flow reactor. The goal of this study was to determine the chain lengthening products from carbon monoxide addition to methanol. To this end reactions were run for 140 minutes at 150 ˚C. This allowed the product composition to

stabilize and be analyzed in steady state. Product analyses were performed on two gas chromatographs: an Agilent 6890 with a wax column (Restek Stabilwax, 30 m, 0.32 mm ID, 1.0 μm film thickness) and a mass sensitive detector (Agilent 5973) was utilized for samples taken with a 25 mL gas tight syringe from a sampling port in the product stream. An Agilent 6850 gas chromatograph with a wax column (Restek Stabilwax, 30 m, 0.32 mm ID, 1.0 μm film thickness) and thermal conductivity detector (TCD) was connected directly to the product stream via a transfer line and a gas-sampling valve. The chromatographic methods and the laminar flow reactor are further described in the supplementary material. Blanks were run with an empty reactor, with a blank silica substrate, and a MoS_2 coated substrate with no gold.

CHAPTER 3: CHARACTERIZATION OF SEAL SWELL UNDER BIO-DERIVED GASOLINE AND DIESEL ANALOG COMPOUNDS

3.1 Introduction

Biofuels have recently emerged as a greener alternative to fossil fuels. Although biofuels are also composed of hydrocarbons, they can be derived from wild vegetation, agricultural crops, or animal waste. Thus, the growth of any plant matter for biofuel production will remove CO_2 from the atmosphere through natural photosynthesis, and will act to reduce net CO_2 emissions. Moving towards biofuels as a potential alternative energy source for automobiles or other transportation, we must assess their compatibility with existing systems. The transition from petroleum-based fuels to biofuels requires testing to guarantee the replacement fuels are sustainable, characterized, and well-suited for the application. It is important to understand the chemical interactions occurring between a new biofuel and any materials in contact in order to decrease negative effects or outcomes. The diversity of biofuels allows their physical properties and composition to be taken into account and then modified, if necessary, to avoid such negative outcomes.

O-ring seals within engines act to prevent fuel leakage but do not maintain optimal function indefinitely. In storage, the shelf life of o-rings range from 3 to 15 years, and for many elastomer types is unlimited. Below, shown in Table 3, is a list of commonly used elastomers for gasket and sealing application. When selecting an effective elastomer material, scientists must take multiple factors into consideration. Service conditions such as operating temperature range, chemical contact, and physical requirements all need to be met.

Table 1. Common elastomers and their properties

Elastomer Type	Application	Density (g/cm^3)
Viton A401C	seal	2.09
Viton B601	seal	2.1
Fluorosilicone	seal	1.77
NBR 1	gasoline dispenser hose	1.46
NBR 2	gasoline dispenser hose	1.52
NBR 3	marine fuel line hose	1.45
NBR 4	small-engine fuel line hose	1.66
NBR 5	gasoline dispenser hose	1.72
NBR 6	tanker-trunk transfer hose	1.74
Neoprene	seal	1.33
Polyurethane	coating	0.97
SBR	cover	1.83
Silicone	seal	1.41

However, this length of time is significantly impacted by environmental conditions such as temperature, humidity, light, radiation, deformation, and contact with liquid, metals, semi-solid materials, and dusting powder. Aromatic hydrocarbons (toluene, benzene, and xylenes) and oxygenated additives (alcohols and ethers) greatly affect the behavior and structure of elastomer seals. Prolonged exposure of elastomers to hydrocarbon fuel results in o-ring volume change, and other dimensional changes. The degree of such changes is a measure of the resistance of the particular elastomer to the fuel. Large volume changes in an o-ring will compromise component functionality. With excessive swelling, an overfilled groove will cause seal failure and leakage. Physical property changes are typically accompanied by an increase in volume, meaning the greater the volume change the greater the change in o-ring thickness, diameter, and mass. It is important to note that some swelling is required to achieve and maintain a seal and to avoid any possibility of leaks. For this reason, high purity biofuel is not used as it may cause the elastomer to shrink. High purity biofuel such as ethanol that is not in a completely sealed environment should not be used due to the propensity for ethanol to absorb moisture from the air, causing water to

build up in the engine. This in turn will lead to poor spark ignition or even corrosion in the fuel tank. The o-rings chosen for these experiments were Viton MIL-PRF-81705D, Type II, Class 1. The size is a standard 2 x 3. Viton was chosen due to its capability of handling a diverse array of applications particularly its great resistance to fuels, oils, and other fluids.

Prolonged exposure of elastomers to biofuels can result in unfavorable polymer/biofuel reactions. The consequences of polymer/biofuel interactions, in this case polymer swelling, can be studied by the Flory-Rehner equation (Equation 1).

$$-[\ln(1-\varphi_2)+\varphi_2+\chi\varphi_2^2]=\rho_2\frac{V_1}{M_c}(1-2\frac{M_c}{M_2})(\varphi_2^{0.333}-\frac{\varphi_2}{2}) \quad (1)$$

Where φ_2 is the volume fraction of polymer in the swollen state ($V_{swollen}/V_{original}=1/\varphi_2$), V_1 the molar volume of solvent, ρ_2 the polymer density, M_2 is the molecular weight, and lastly M_c is the molecular weight of chains between crosslinks [https://www.stevenabbott.co.uk/practical-solubility/polymer-swelling.php]. The Flory-Rehner equation relates polymer swelling to the molecular weight of chains between crosslinks. Two major factors that relate to the degree of swelling are the solubility of the polymer in the solvent and the length of chains between crosslinks. Polymer-fuel favored interactions will lead to large swelling whereas polymer-polymer interactions will lead to shrinking of the elastomer.

This study will investigate the degradation and swelling characteristics of Viton o-ring seals after continuous contact with singular (unblended) biofuel compounds. Many of the compounds tested differ from conventional gasoline and diesel fuels and have not been previously investigated with the intention of compatibility with modern engines.

3.2 Experimental

3.2.1 Gasoline and Diesel Analog Compounds

The fuel compounds chosen were not combined into mixtures but tested individually. The bio-gasoline compounds were ethanol, cyclopentanone, methyl acetate, ethyl acetate, 2-methylfuran, and diisobutylene. The bio-diesel compounds tested were 1-nonanol, butylcyclohexane, dibutoxymethane, n-dodecane, and dodecanes. Their chemical structures are shown in Tables 1 and 2 below.

Table 2. Functional groups and chemical structures of bio-gasolines investigated.

Bio-Gasoline	Functional Group	Chemical Structure
Ethanol	Alcohol	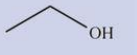
Cyclopentanone	Ketone	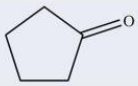
Methyl Acetate	Ester	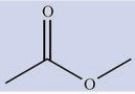
Ethyl Acetate	Ester	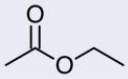
2-Methylfuran	Ether	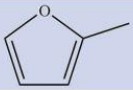
Diisobutylene	Olefin	

Table 3. Functional groups and chemical structures of bio-diesels investigated.

Bio-Diesel	Functional Group	Chemical Structure
1-Nonanol	Alcohol	
Butylcyclohexane	Cyclic Alkane	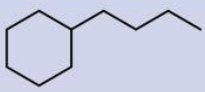
Dibutoxymethane	Acetal	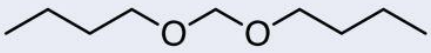
n-Dodecane	Linear Alkane	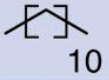

3.2.2 ASTM Procedure

For each of the liquid hydrocarbon compounds chosen, standard 2 x 3 viton o-rings were submerged in a separate test tube. O-rings were threaded onto a thin wire, spaced apart by glass

beads to prevent elastomer contact, and then submerged as a unit in a single biofuel compound as shown in Figure 6. The glass beads were made of agate material, as known as silicon dioxide, which was used because it is inert in the system. To obtain good standard deviation, short-term submersion studies utilized 5 o-rings per test tube, whereas 10 were submerged for long-term studies.

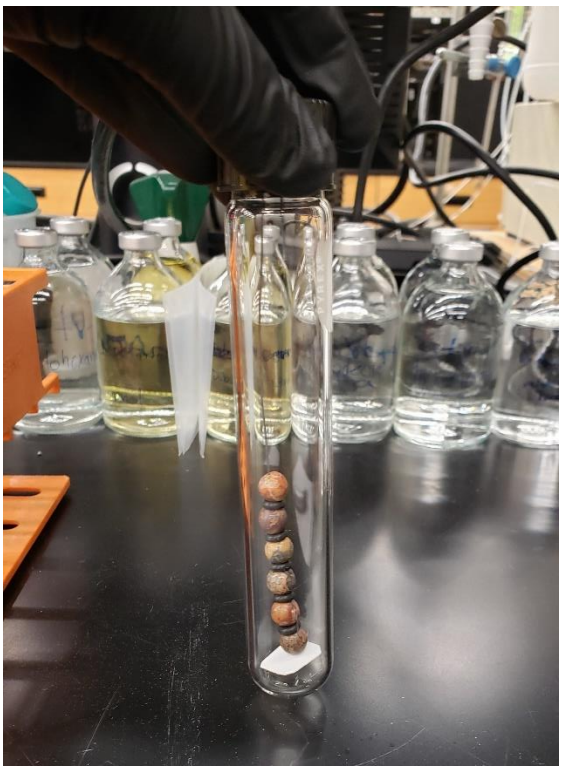

Figure 6. The placement of o-rings in each test tube prior to filling with liquid fuel.

Mass, density, thickness, and diameter measurements of each o-ring were taken prior to submersion, and again after different lengths of time of submersion. Short-term studies included o-ring measurements after each hour submerged in liquid, for up to 6 hours. Long-term studies had measurements conducted every few days, and time between measurements increased after months

of submersion. Care is taken to ensure o-rings remained outside the fuel bath for as little time as possible. While one o-ring is undergoing measurement, the rest are held submerged in fuel.

3.2.2.1 Quantification of Mass

One o-ring was removed from the fuel and wire at a time, rinsed briefly in acetone and gently wiped to remove fuel and any liquid droplets. It was then placed in a tared weigh bottle and massed on a Mettler AT20 micro-balance with a range from 2 µg to 22 g (Figure 7). If the o-ring experiences gradual evaporation of fuel, despite being washed, the first stable mass is recorded.

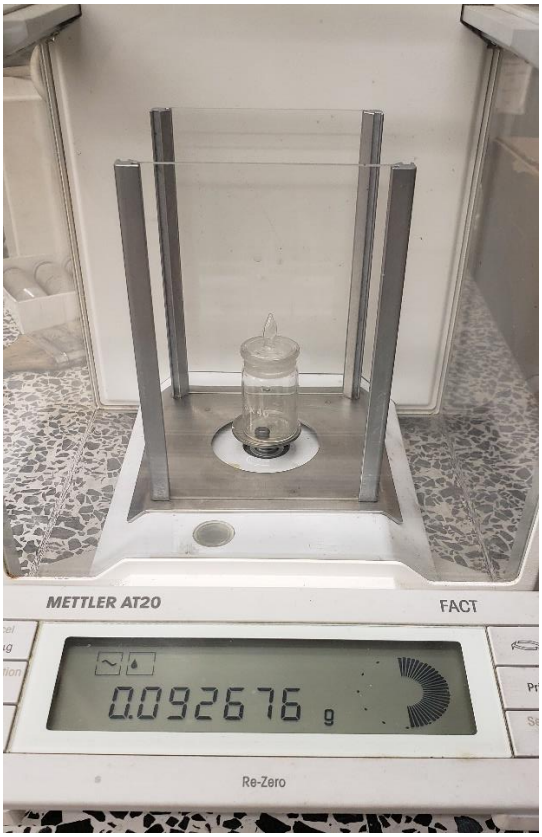

Figure 7. Mass determination of each o-ring based on ASTM procedure.

3.2.2.2 Quantification of Density

After the mass measurement, the o-ring is moved to a standard mass balance, fitted with a rig designed to measure water-submerged mass (Figure 8). A platform is placed around the weighing tray to hold a jacketed water bath without contributing to the mass measurement. Inside the jacket, coolant flows through an inlet and outlet from a chiller held at 25 °C, maintaining the water bath at roughly room temperature.

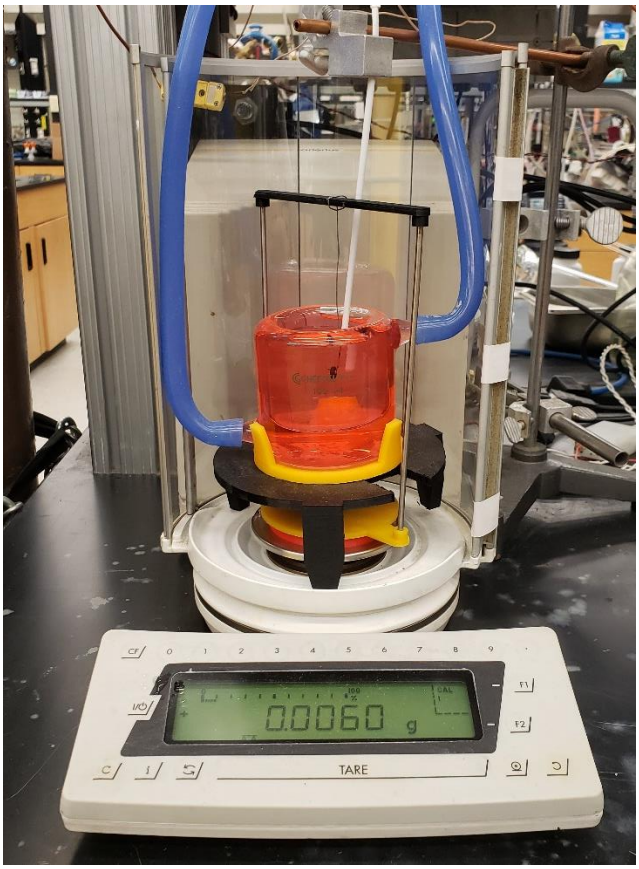

Figure 8. A mass measurement of each o-ring is taken while submerged in distilled water.

A scaffold resting on a Sartorius MC4108 balance tray reaches above the bath, holding a hook upon which each o-ring is placed. The balance has a range of 2 µg to 21g, and ±1 ppm/°C sensitivity. This scaffold and hook is tared, while some of the hook is submerged at the current

water level. Then, the o-ring is placed on the hook, enabling the recorded mass to reflect only the elastomer itself. After removing from the water bath, the o-ring is dipped briefly in acetone and wiped to remove all traces of liquid.

3.2.2.3 Quantification of Dimensional Change

Thickness and diameter of the o-rings were determined by a Starrett No. 796XFL-1 digital micrometer with a range of 0 – 25 mm, resolution of 0.001 mm, and an accuracy of ±0.002 mm. At this stage, damage to the o-ring is assessed before quickly replacing the o-ring in a new test tube containing the same fuel. Once all of the parameters were recorded such as mass of the o-ring in air, mass of the o-ring submerged, temperature of the bath in °C, thickness, and diameter, the volume change was then calculated using Equations 2 and 3.

$$Volume_{o-ring} = \frac{(Mass_{air,grams} - Mass_{submerged,grams})}{Density_{water}} \quad (2)$$

$$Volume_{avg} = \frac{Volume_{o-ring,1} + Volume_{o-ring,2} + \cdots Volume_{o-ring,nth}}{n} \quad (3)$$

To better understand the results presented in the following section, a table showing the boiling point and molecular weight of each gasoline and diesel compounds are listed below in Tables 4 and 5. This will help relate the mass and how the evaporation of certain fuels affects the measured mass, thickness, and diameter of the o-rings.

3.3 Results

3.3.1 Long-Duration ASTM Procedure

The o-rings were submerged in each bio-gasoline compound for approximately 365 days, and 250 days for bio-diesel. As shown in Figures 9-16, the bulk of the swelling occurred during the first few days. The most damaging fuel to the elastomer was cyclopentanone in terms of mass gain, and overall size increase. However, similar results were found with methyl and ethyl acetate, which are observed to have comparable negative structural changes. The least significant swelling occurred for ethanol and diisobutylene, with the latter having slightly less of an impact overall. These two gasoline compounds showed results close to that of the diesel fuels in terms of their resistivity. 2-Methylfuran produced a somewhat intermediate result, though is not as severe of a swell as cyclopentanone or the acetate compounds.

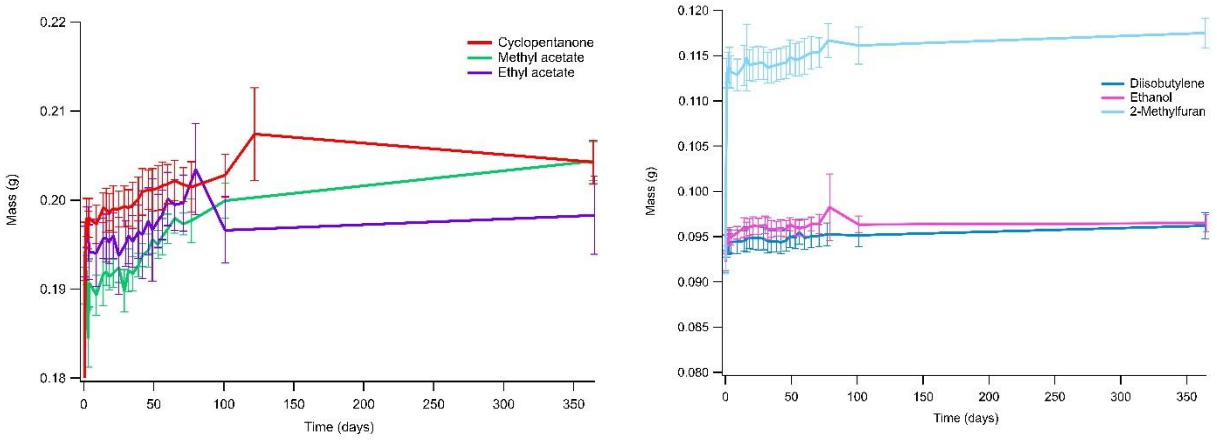

Figure 9. Changes in mass for long-term measurements of gasoline compounds.

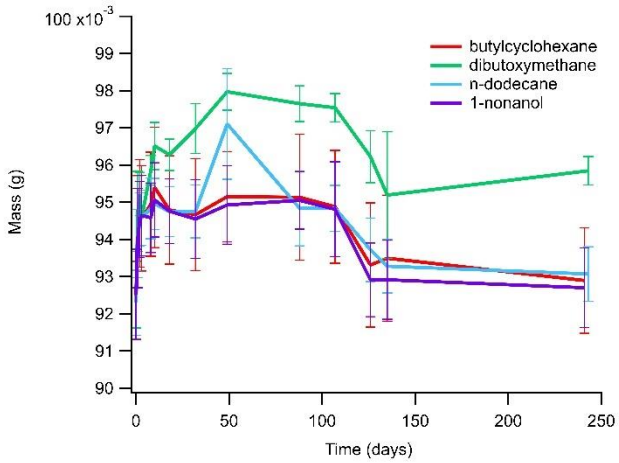

Figure 10. Changes in mass for long-term measurements of diesel compounds.

Upon initial submersion the o-rings experienced the most severe swelling, which proceeded on the order of hours. Then, more gradual swelling continues for approximately 100 days before the fuel has likely permeated the o-ring completely and the dimensional changes plateau.

Rapid measurement of the mass, volume, thickness, and diameter was required due to the volatility of the fuels. As the o-rings were transferred from the fuel into air, in many cases absorbed fuel from within the o-rings slowly began to evaporate, resulting in mass fluxuations. The degree of these fluctuations are illustrated with error bars in Figures 9-19. The last measurements taken (thickness and diameter) will differ most from the conditions of submersion since the o-rings were exposed to air for a longer duration than the measurements taken prior. Implementation of *in-situ* seal swell measurements to the ASTM procedure should significantly increase the overall accuracy of these measurements.

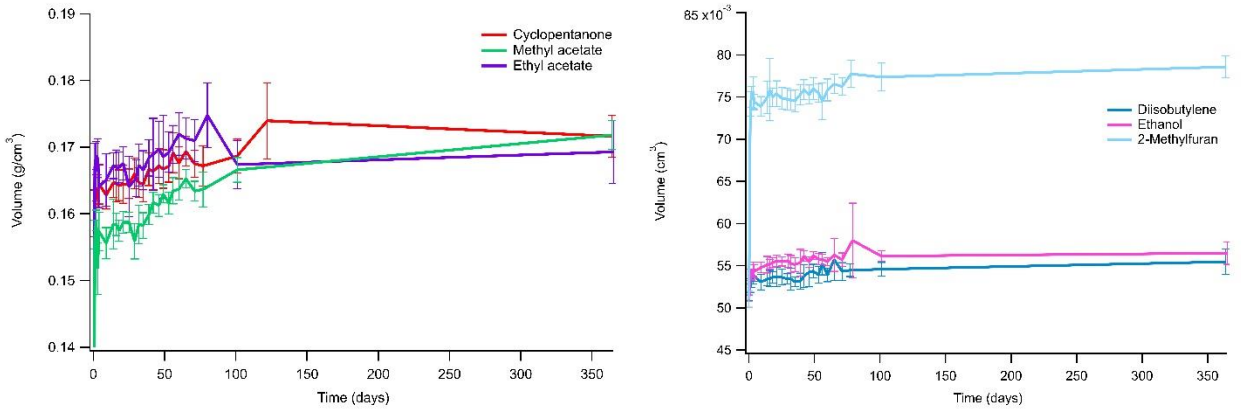

Figure 11. Changes in volume for long-term measurements of gasoline compounds.

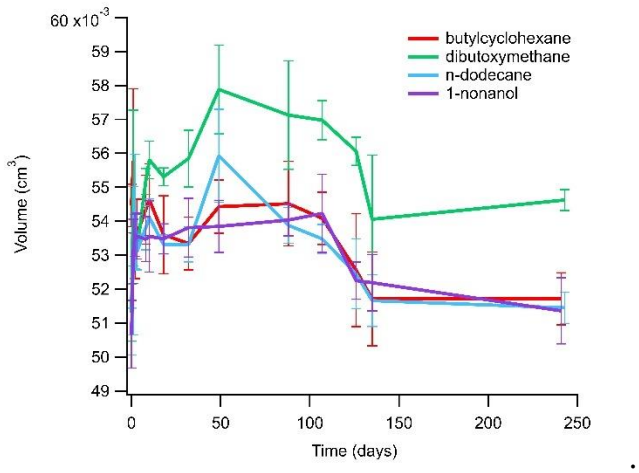

Figure 12. Changes in volume for long-term measurements of diesel compounds.

Diesel possesses a higher viscosity than gasoline, causing diesel evaporation at slower rates than that of the gasoline when in contact with the elastomer. Unlike the differences in degree of swelling seen among bio-gasoline compounds, bio-diesel exhibited similar results to one another (Figures 10, 12, 14, 16). Each of the diesel fuels, butylcyclohexane, dibutoxymethane, n-dodecane, and 1-nonanol all had a minor impact on the swelling of the o-rings, with dibutoxymethane being

the highest of the four fuels tested. One can also see that after approximately 120 to 130 days the swelling of the o-rings begins to plateau.

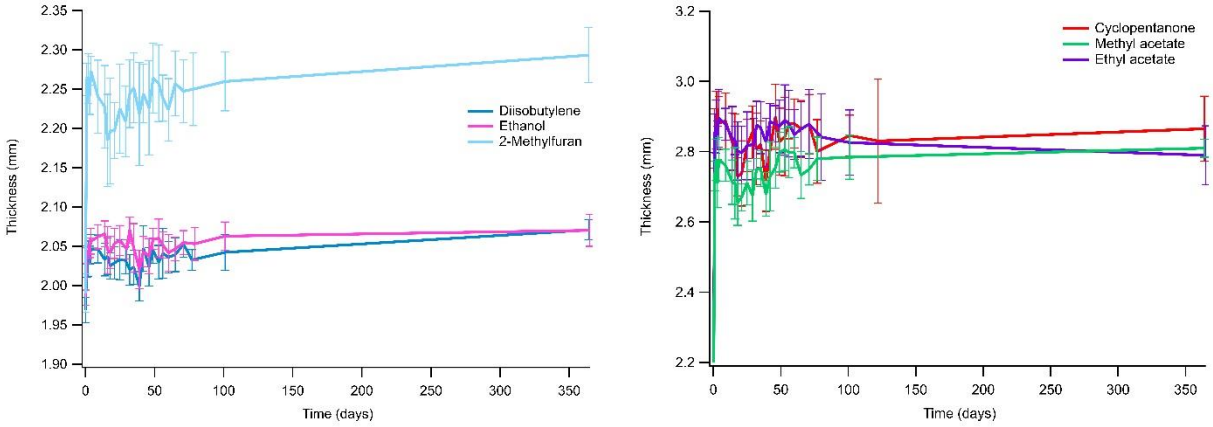

Figure 13. Changes in thickness for long-term measurements of gasoline compounds.

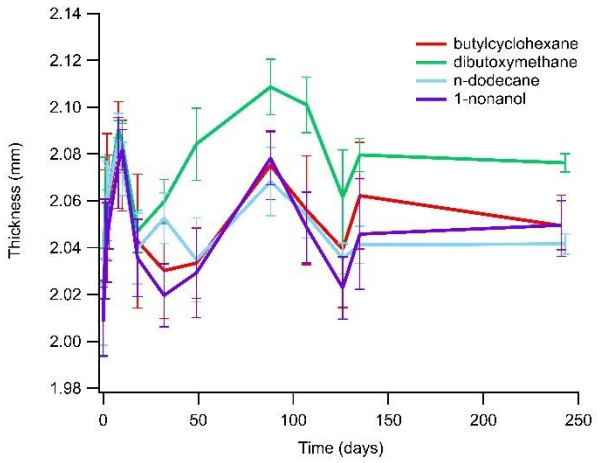

Figure 14. Changes in thickness for long-term measurements of diesel compounds.

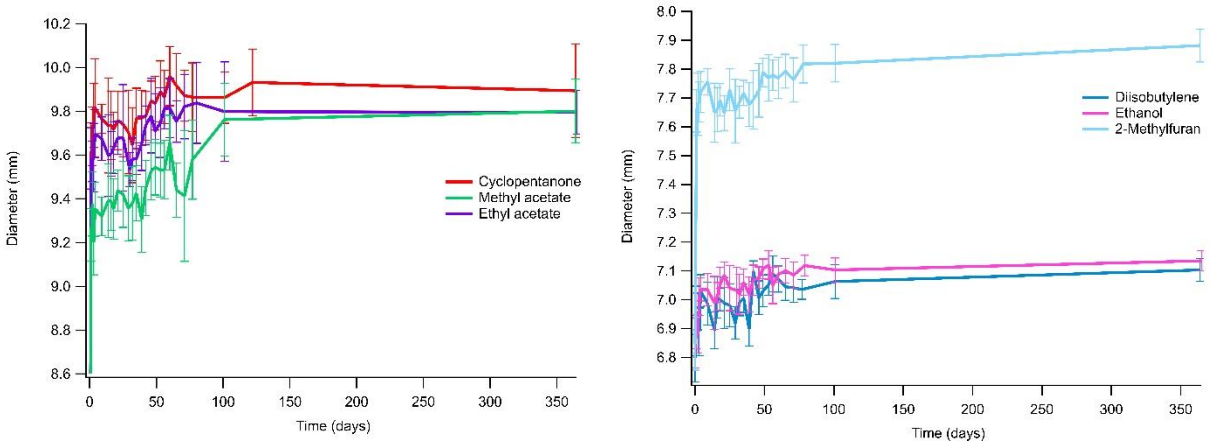

Figure 15. Changes in diameter for long-term measurements of gasoline compounds.

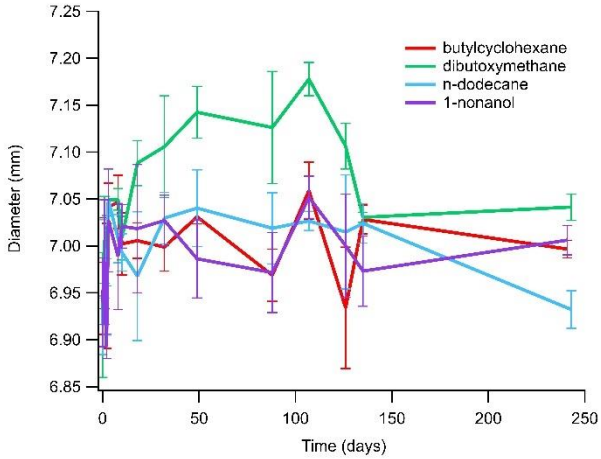

Figure 16. Changes in diameter for long-term measurements of diesel compounds.

3.3.2 Short-Duration ASTM Procedure

As discussed, the bulk of swelling occurs in the first few hours of submersion. Thus, to have a better understanding of what occurred during the first few hours of contact with the fuel, short-duration experiments were conducted (Figures 17-19). Since the majority of the changes occurred in this time frame, it is desired to get as detailed a representation of the elastomer swelling as possible. In this set of experiments, dodecanes was added to the diesel fuels tested.

Measurements of mass, volume, thickness, and diameter were taken every hour up to six hours. Five o-rings were used for this part of the analysis rather than 10, which was needed to adjust for the shorter time intervals between fuels.

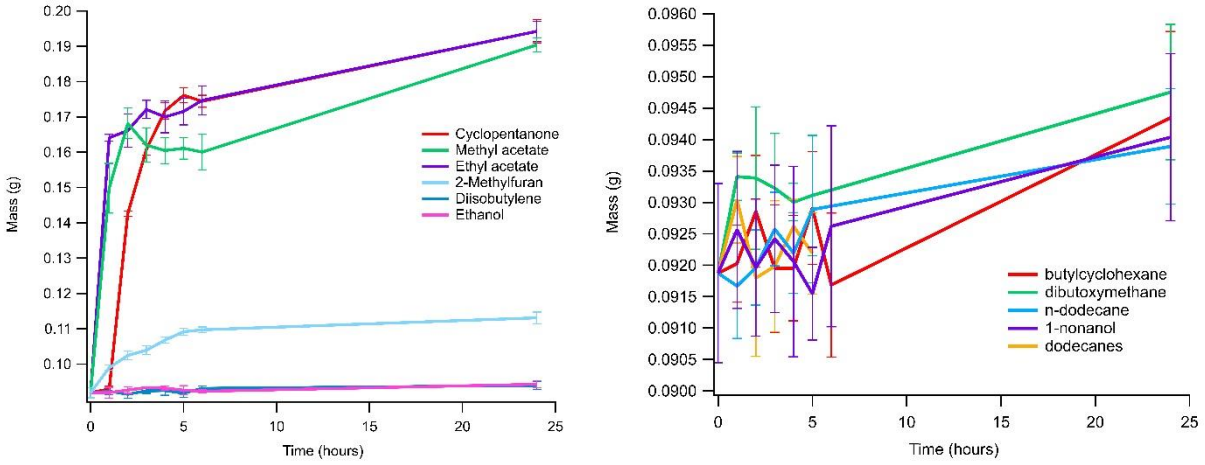

Figure 17. Changes in mass over a 24 hour period for gasoline and diesel compounds.

It was observed that for gasoline compounds, the largest swelling and mass gain occurred in as early as the first hour. Diesel compounds showed more gradual swelling over the 24 hour period. Even so, all diesel compounds have proven more resistant to swelling than gasoline even after a day submerged.

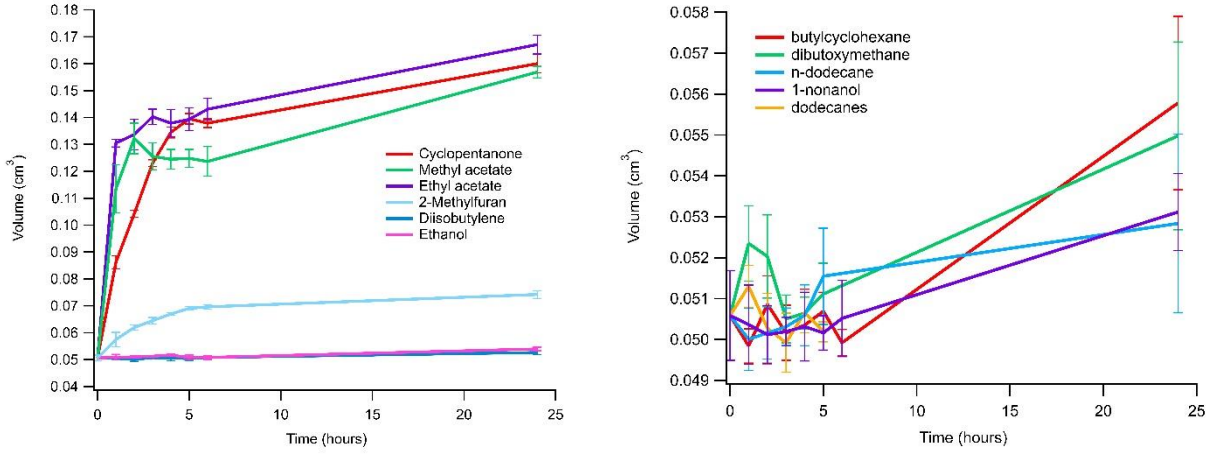

Figure 18. Changes in volume over a 24 hour period for gasoline and diesel compounds.

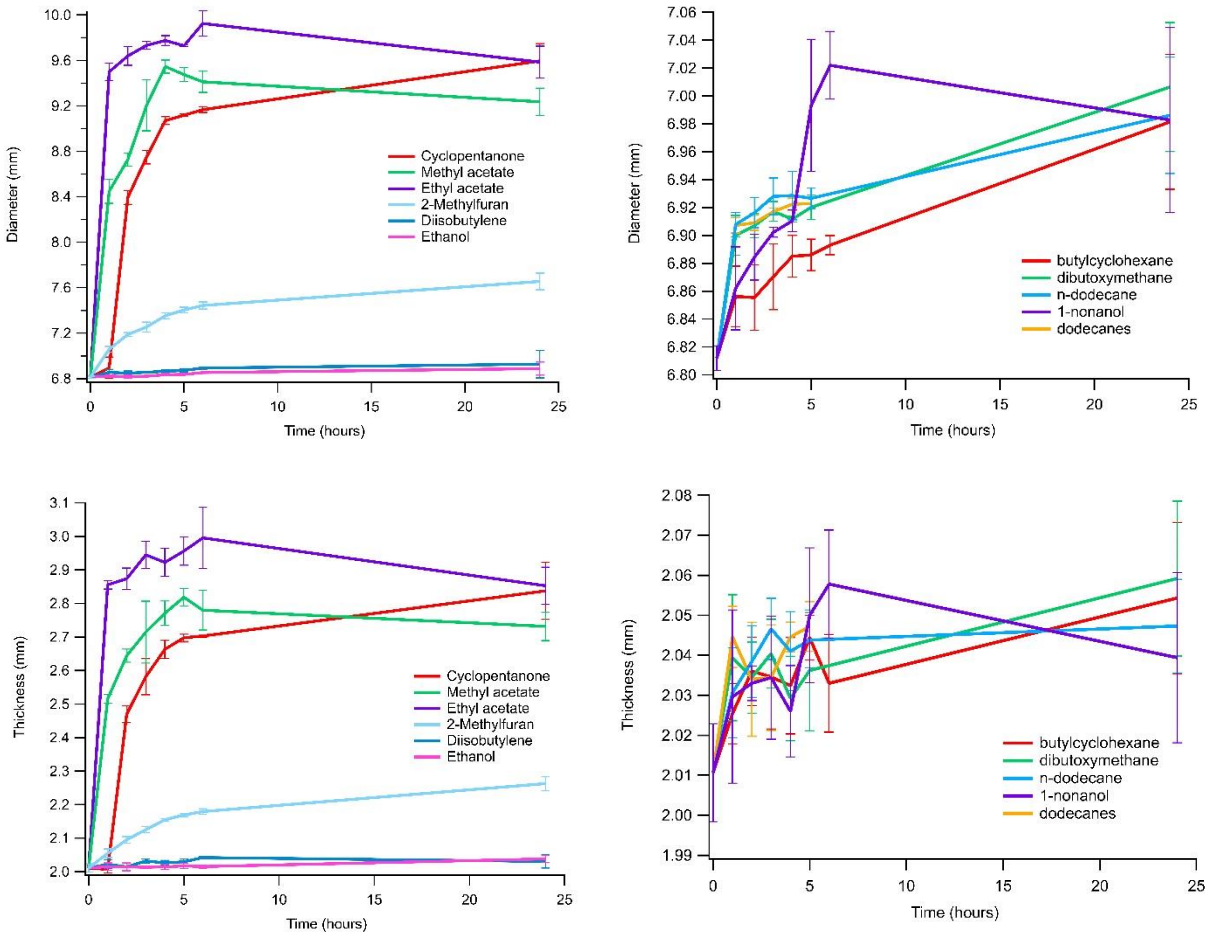

Figure 19. Changes in thickness and diameter over a 24 hour period for gasoline and diesel compounds.

3.4 Discussion

Analysis showed that the swelling behavior can be attributed to the polarity of the fuels. Typically, the performance of the elastomer will correspond more with polarity than with hydrogen bonding[61]. The swelling and mass increase of the o-rings will depend on the elastomer material type used. Viton is known to be resistant to a wide range of chemicals, particularly ketones, esters and chemicals of high polarity. Diisobuytlene and ethanol showed the lowest swelling due to having the lowest polarity of the gasoline fuels chosen (Tables 4 and 5). The lower resistance of cyclopentanone to swelling is likely due to its being a largely polar molecule. The greater swelling

over the other gasoline fuels indicates that its polarity is more predominant than the hydrogen bonding in the other fuels. Hydrogen bonding occurs primarily near oxygen atoms; as a result, the forces coupled with hydrogen bonding are more local. The potential for polar attraction on the polymer molecule chains orients the fuel molecules in such a way that an interference is caused with the hydrogen bonding potential of the oxygen atoms, leading to low swelling.

Table 4. Properties of gasoline compounds

Gasoline Compounds	Chemical formula	BP °C	MW (g/mol)	ρ_{25C} (g/mL)	ε_{25C}	Functional Group
Cyclopentanone	C_5H_8O	130 - 131	84.12	0.951	13.52	Ketone
Diisobutylene	C_8H_{16}	101 - 103	112.21	0.716	-	Olefin
Methyl acetate	$C_3H_6O_2$	57 - 58	74.08	0.932	6.68	Ester
2-Methylfuran	C_5H_6O	63 - 66	82.1	0.91	-	Ether
Ethanol	C_2H_6O	78	46.068	0.789	24.3	Alcohol
Ethyl acetate	$C_4H_8O_2$	76.5 - 77.5	88.11	0.902	6.02	Ester

Table 5. Properties of diesel compounds

Diesel Compounds	Chemical formula	BP °C	MW (g/mol)	ρ_{25C} (g/mL)	ε_{20C}	Functional Group
1-Nonanol	$C_9H_{20}O$	215	144.25	0.827	9.09	Alcohol
Butylcyclohexane	$C_{10}H_{20}$	178 - 180	140.27	0.818	-	Cyclic Alkane
Dibutoxymethane	$C_9H_{20}O_2$	180	160.25	0.84	-	Acetal
N-dodecane	$C_{12}H_{26}$	216.3	170.33	0.75	2.012	Linear Alkane
Dodecanes	$C_{12}H_{26}$	215 - 217	170.33	0.75	2.01	Linear Alkane

Diesel is typically a heavier fluid than gasoline since it is composed of larger molecules. We might expect that the o-rings submerged in higher molecular weight compounds would result in a larger gain in mass. However, we have found that the results seem largely independent of the molecular weights of the compounds (reported in Tables 4 and 5). The dielectric constant ("ε"), or permittivity, is a measure of the polarity of the solvent or fluid. The higher the dielectric constant the higher the polarity of the molecule. Polar solvents have typically $\varepsilon > 20$ whereas nonpolar solvents have $\varepsilon < 20$. Tables 4 and 5 show the values of each fuel's dielectric constant.

3.5 Conclusion

The goal of this study was to analyze the compatibility of renewable fuels for elastomers in specific o-rings. It is important to move toward biofuels as a potential alternative energy source for automobiles or other methods of transportation as it serves as a more green energy source. Two fossil fuel alternatives were studied and their results reported, such as properties of biofuels and hydrocarbon synthesis from syngas. An important factor when investigating these fuel alternatives is the longevity of elastomers when submerged with a fuel. As reported in the findings above, within the first few hours o-rings begin to swell and deform, making a leak in the system possible. It is important to test the compatibility of the bio-derived fuels with elastomers before completely switching to this as a form of transportation of vehicles.

Finding alternative fuel options has proven to be a massive undertaking to successfully make the swap, so there is an abundance of future work that may be performed to expand on the research and results already found. Future work includes removing the current ASTM procedure and replacing it with an improved ASTM procedure that will allow for real time measurements as the elastomer remains submerged. This will allow for significantly more accurate results, leading to a much smaller standard deviation as well as a decrease in percent error reported above. A possible method to improve the measurement of seal swell in real time would be to use a piezoelectric material in concurrence with a speed of sound instrument. Using this, one could measure the o-rings while submerged, and never need to remove the o-ring from the fuel bath. This new method will allow us to numerically see the o-ring swell within the first few hours without the o-ring shrinking back to its original shape and size when exposed to air. This detail is instrumental to overall success and accuracy as this will show if an o-ring will soon fail. Since damages can be observed without removing the o-ring from the entire system, leaks and overall

failures can be prevented. Lastly, with this new method information on how long an o-ring will last in a certain system will give more accurate data on the longevity and performance of the o-ring.

CHAPTER 4: CONCLUSION

Two methodologies of testing the mass, volume, thickness, and diameter was done for both short duration submersion as well as long duration submersion. Each of these methods of testing showed similar results in that the swelling occurred during the first few hours. It is safe to say that only using the short duration method works for establishing compatibility for biofuels with the chosen elastomer. Although each of the methodologies resulted in similar results, more information on the elastomer can be gathered by studying the long duration method. After a certain amount of time, in this case days, swelling of the o-ring begins to stop. During this time cracks and ragged edges are visible, as well as very small pieces of the o-ring floating within the fuel. To see the physical damage done to the o-ring the long duration experiments represent that effectively.

APPENDIX
SUPPLEMENTAL INFORMATION FOR CHAPTER 2

Experimental

Gas chromatography

Mass Sensitive Detection (GC-MS) was performed on an Agilent 6890 GC with Agilent 5973 mass sensitive detector. The m/z range was set to 6-550 amu. A Restek Stabilwax column (30, 0.32 mm ID, 1.0 µm film thickness) was used for separation. 25 µL samples were taken from a sampling port on the reactor transfer line. The analysis parameters were:

Oven	*Front Inlet (Split/Splitless)*	*Post Run*
Mode: constant flow Initial flow: 1.5 mL/min Initial temp: 40 ˚C Initial time: 1.00 min Ramps: # Rate Final temp Final time 1 30.00 225 5.00 Post temp: 235 ˚C Post time: 2.00 min Run time: 12.17 min	Mode: Splitless Initial temp: 150 ˚C Pressure: 1.71 psi Purge flow: 15.0 mL/min Purge time: 2.00 min Gas type: Helium	Post Time: 2.00 min Oven Temperature: 235 ˚C Column 1 Flow: 1.5 mL/min

Thermal Conductivity Detection (GC-TCD) was performed on an Agilent 6850 GC with TCD detector and gas sampling valve. The product stream was fed to the gas sampling valve by a 366 cm unheated 0.3175 cm OD, 0.2159 cm ID stainless steel transfer line with a total volume of 13.4 cm^3. A Restek Stabilwax column (30, 0.25 mm ID, 1.00 µm film thickness) was used for separation. Samples were automatically taken at 30 minute intervals vial gas-sampling valve.

Oven
Mode: constant flow Initial flow: 1.5 mL/min Initial temp: 40 ˚C Initial time: 1.00 min Ramps: # Rate Final temp Final time 1 30.00 225 5.00 2 0.0(Off) Post temp: 235 ˚C

Post time: 2.00 min
Run time: 12.17 min

Plug Flow Reactor

Figure 20 shows an exploded view of the reactor with a sapphire window. Maximum operational temperature is 250 ˚C and maximum operational pressure is 2.5 MPa. The plug flow reactor is constructed of 316L stainless steel with high-pressure inlet and outlet fittings. Temperature control is achieved with a cartridge heater (S1 front left), RTD sensor (S1 rear left), and a process controller (Omega CN7800 series) with SCR control. Reactants enter the reaction chamber from the bottom of the center of the circular pocket and exit the side. A porous sintered stainless steel disk supports the catalyst sample during operation to distribute the reactant stream.

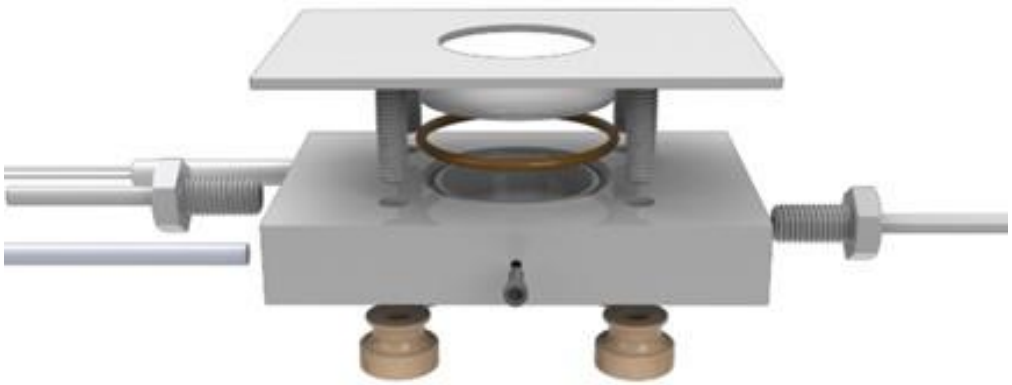

Figure 20. An exploded view of the plug flow reactor. It can be easily loaded under oxygen and water free conditions in a glove box.

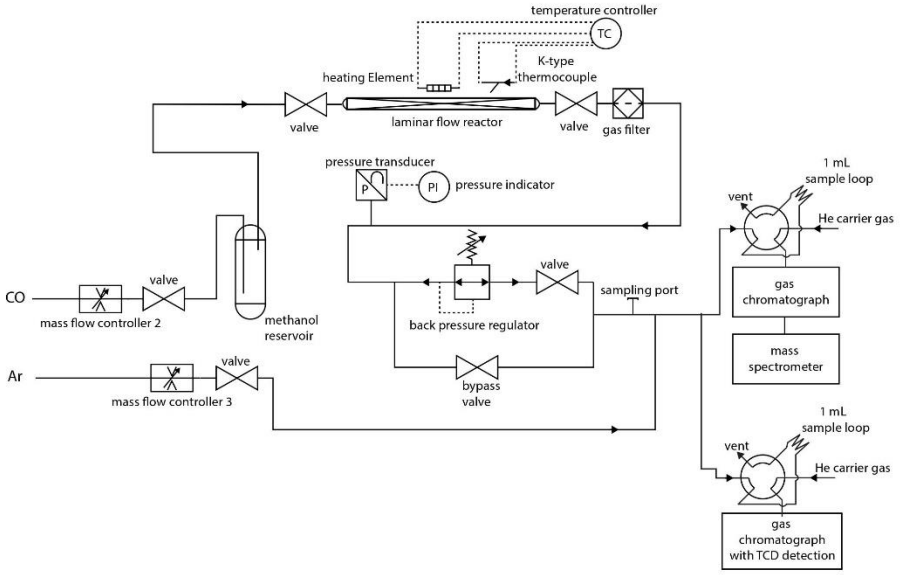

Figure 21. The reactor system consists of two mass flow controllers (Tylan, 0-50 SCCM for CO and 0-10 sccm for other gases). A liquid reservoir (right) fitted with a sparge serves as a bubbler to produce a feed stream saturated with reactant vapor. A backpressure regulator (left, 0 to 792 kPa) allows higher pressure to be realized in the reaction chamber (center). Valves before and after the reaction chamber allow it to be loaded under inert conditions and put on test without compromising the integrity of the catalyst.

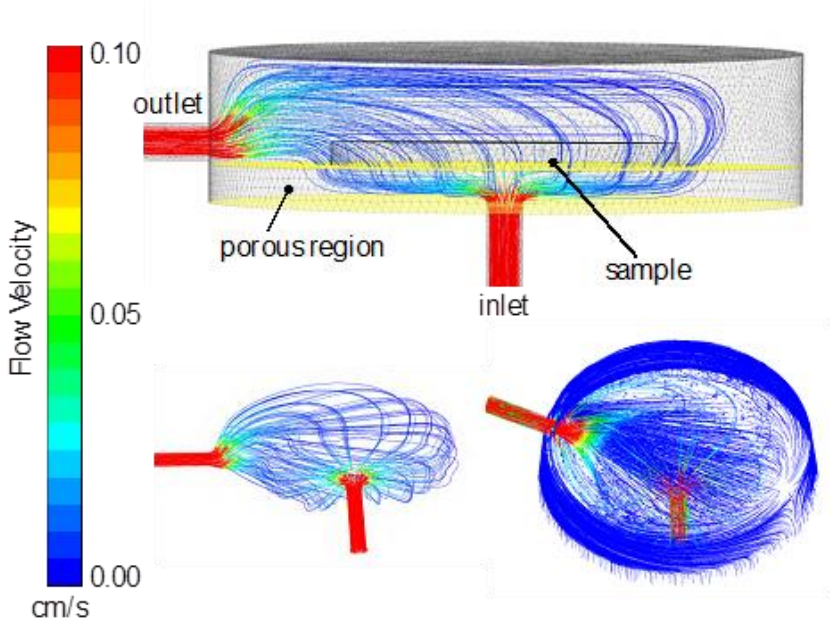

Figure 22. Reactant flow around the sample occurs with a uniform velocity after passing though a porous region and impinging on the bottom of the sample.

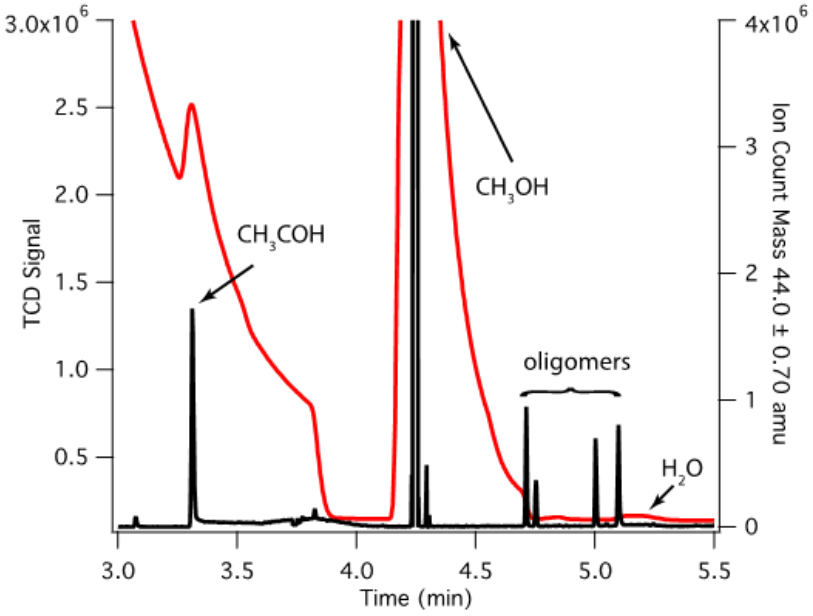

Figure 23. The thermal conductivity data from CO+methanol over 1 Å gold on single layer MoS_2, after 97 minutes on stream shows acetaldehyde at 3.305 min, methanol at 4.245 min, and water at 5.149 min. For comparison, a GC-MS chromatogram of a standard in selected ion mode (mass=44) is overlaid. The standard was sampled from the vapor-saturated headspace of a methanol/acetaldehyde mixture.

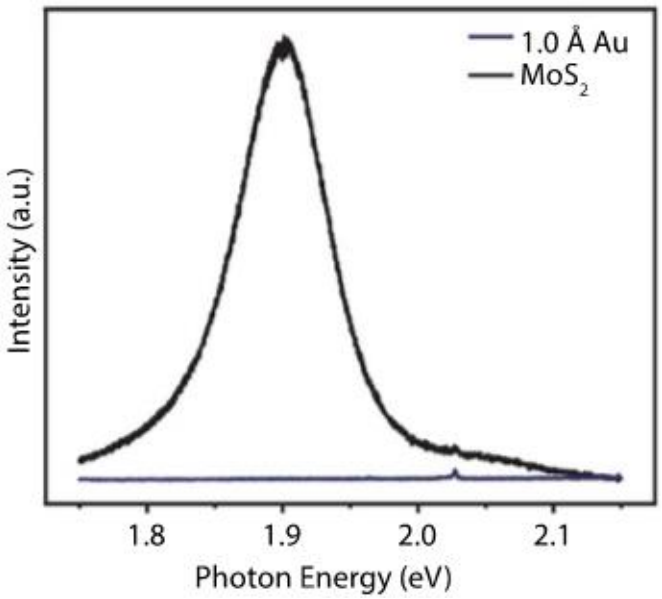

Figure 24. The photoluminescence of the deposited MoS_2 film before (black) and after gold deposition (blue) shows quenching by the gold particles and is used is a verification of deposition as well as homogeneity.

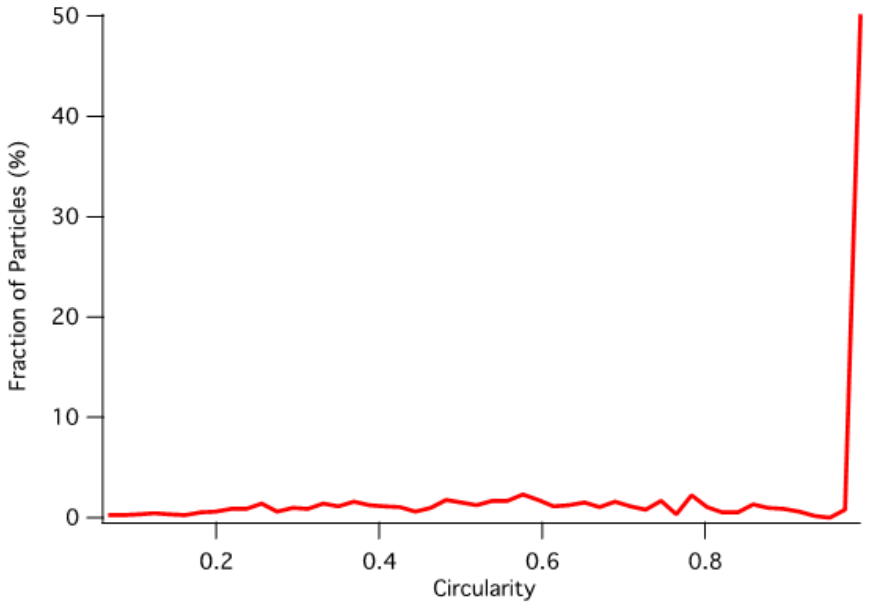

Figure 25. Before use, the gold particles on the substrate are mostly circular with the majority of the circularity (4π(area/perimeter^2)) near unity.

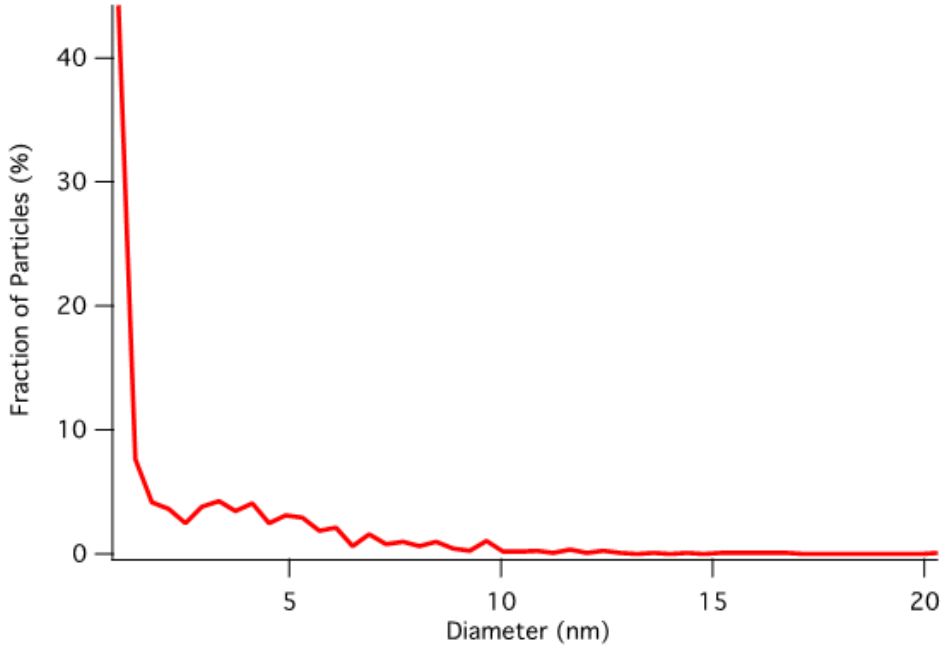

Figure 26. Before use, the gold particles range from 1-5 nm in diameter with a near exponential distribution suggestion random nucleation events.

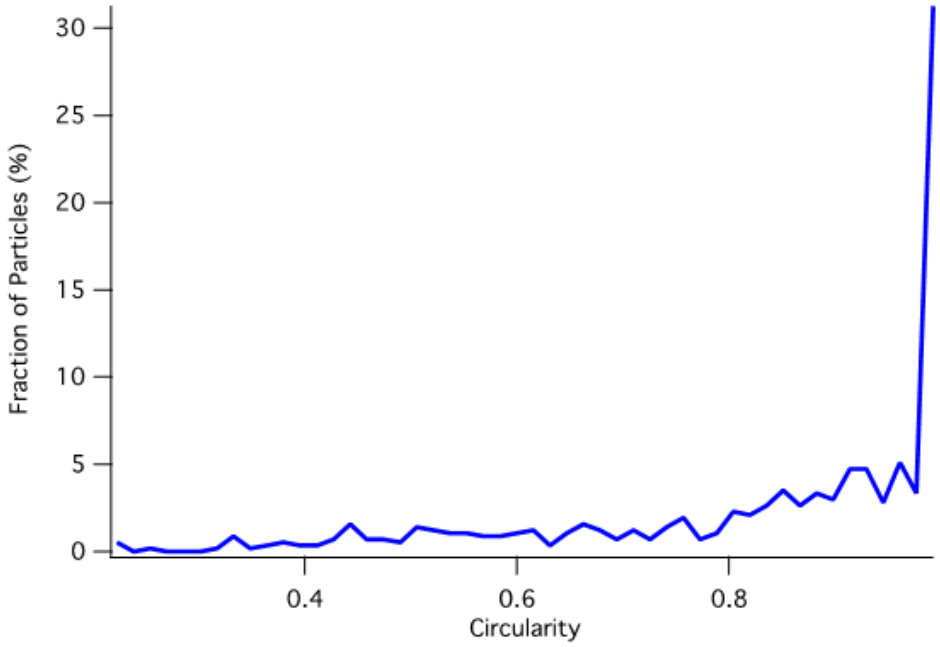

Figure 27. After use, the gold particles on the substrate coalesced. While the majority of the circularity (4π(area/perimeter^2)) is still near unity, a significant fraction shows deviation toward elliptical shapes.

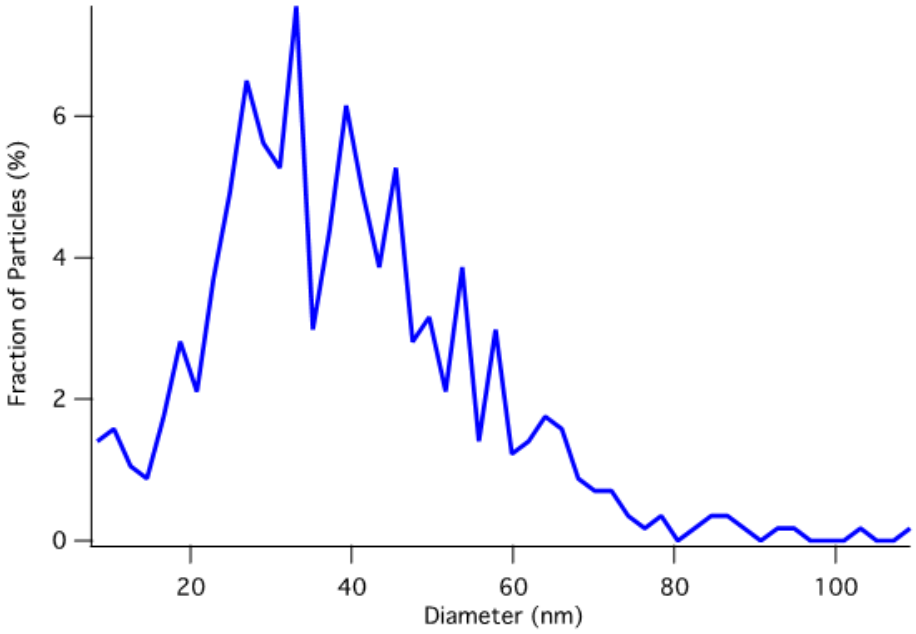

Figure 28. After use, the gold particles coalesced with a diameter distribution centered near 40 nm. The change in distribution to an exponentiall modified Normal distribution suggests the coalescing proceeds through though Ostwald ripening mechanism.

LIST OF REFERENCES

[1] 2020, "What is U.S. electricity generation by energy source?," https://www.eia.gov/tools/faqs/faq.php?id=427&t=3.

[2] Levin, K., 2018, "According to New IPCC Report, the World is on Track to Exceed its "Carbon Budget" in 12 Years," https://www.wri.org/blog/2018/10/according-new-ipcc-report-world-track-exceed-its-carbon-budget-12-years.

[3] Robert C. Ketcham, e. a., 1986, "Investigation of the Challenger Accident," Committee on Science and Technology House of Representatives.

[4] Heitzig, S., Weinebeck, A., and Murrenhoff, H., 2015, "Testing and Prediction of Material Compatibility of Biofuel Candidates with Elastomeric Materials," SAE International Journal of Fuels and Lubricants, 8(3), pp. 549-559.

[5] Grim, R. G., To, A. T., Farberow, C. A., Hensley, J. E., Ruddy, D. A., and Schaidle, J. A., 2019, "Growing the Bioeconomy through Catalysis: A Review of Recent Advancements in the Production of Fuels and Chemicals from Syngas-Derived Oxygenates," ACS Catalysis, 9(5), pp. 4145-4172.

[6] Bai, H., Ma, M., Bai, B., Cao, H., Zhang, L., Gao, Z., Vinokurov, V. A., and Huang, W., 2019, "Carbon chain growth by formyl coupling over the Cu/γ-AlOOH(001) surface in syngas conversion," Physical Chemistry Chemical Physics, 21(1), pp. 148-159.

[7] Choi, Y., and Liu, P., 2009, "Mechanism of Ethanol Synthesis from Syngas on Rh(111)," Journal of the American Chemical Society, 131(36), pp. 13054-13061.

[8] Haruta, M., Kobayashi, T., Sano, H., and Yamada, N., 1987, "Novel Gold Catalysts for the Oxidation of Carbon-Monoxide at a Temperature Far Below 0-Degrees-C," Chemistry Letters(2), pp. 405-408.

[9] Hammer, B., and Norskov, J. K., 1995, "Why gold Is the noblest of all the metals," Nature, 376(6537), pp. 238-240.

[10] Rawal, T. B., Le, D., and Rahman, T. S., 2017, "Effect of single-layer MoS_2 on the geometry, electronic structure, and reactivity of transition metal nanoparticles," Journal of Physical Chemistry C, 121(13), pp. 7282-7293.

[11] Almeida, K., Pena, P., Rawal, T. B., Coley, W. C., Akhavi, A.-A., Wurch, M., Yamaguchi, K., Le, D., Dowben, P. A., Rahman, T. S., and Bartels, L., 2019, "A Single-Layer of MoS_2 activates Gold for Room Temperature CO Oxidation on an Inert Silica Substrate," Journal of Physical Chemistry C, 123 (11), pp. 6592–6598.

[12] Haruta, M., Tsubota, S., Kobayashi, T., Kageyama, H., Genet, M. J., and Delmon, B., 1993, "Low-temperature oxidation of CO over gold supported on TiO_2, alpha-Fe_2O_3, and Co_3O_4," Journal of Catalysis, 144(1), pp. 175-192.

[13] Schubert, M. M., Plzak, V., Garche, J., and Behm, R. J., 2001, "Activity, selectivity, and long-term stability of different metal oxide supported gold catalysts for the preferential CO oxidation in H-2-rich gas," Catalysis Letters, 76(3-4), pp. 143-150.

[14] Deng, W. L., De Jesus, J., Saltsburg, H., and Flytzani-Stephanopoulos, M., 2005, "Low-content gold-ceria catalysts for the water-gas shift and preferential CO oxidation reactions," Applied Catalysis, A291(1-2), pp. 126-135.

[15] Gardner, S. D., Hoflund, G. B., Schryer, D. R., Schryer, J., Upchurch, B. T., and Kielin, E. J., 1991, "Catalytic Behavior of Noble-Metal Reducible Oxide Materials for Low-

Temperature Co Oxidation .1. Comparison of Catalyst Performance," Langmuir, 7(10), pp. 2135-2139.
[16] Chen, M. S., and Goodman, D. W., 2004, "The structure of catalytically active gold on titania," Science, 306(5694), pp. 252-255.
[17] Zhou, Y. Y., Lawrence, N. J., Wang, L., Kong, L. M., Wu, T. S., Liu, J., Gao, Y., Brewer, J. R., Lawrence, V. K., Sabirianov, R. F., Soo, Y. L., Zeng, X. C., Dowben, P. A., Mei, W. N., and Cheung, C. L., 2013, "Resonant Photoemission Observations and DFT Study of s-d Hybridization in Catalytically Active Gold Clusters on Ceria Nanorods," Angewandte Chemie-International Edition, 52(27), pp. 6936-6939.
[18] Yang, F., Graciani, J., Evans, J., Liu, P., Hrbek, J., Sanz, J. F., and Rodriguez, J. A., 2011, "CO Oxidation on Inverse CeO(x)/Cu(111) Catalysts: High Catalytic Activity and Ceria-Promoted Dissociation of O(2)," Journal of the American Chemical Society, 133(10), pp. 3444-3451.
[19] Merida, C. S., Le, D., Echeverria, E. M., Nguyen, A. E., Rawal, T. B., Alvillar, S. N., Kandyba, V., Al-Mahboob, A., Losovyj, Y., Katsiev, K., Valentin, M. D., Huang, C. Y., Gomez, M. J., Lu, I. H., Guan, A., Barinov, A., Rahman, T. S., Dowben, P. A., and Bartels, L., 2018, "Gold Dispersion and Activation on the Basal Plane of Single-Layer MoS_2," Journal of Physical Chemistry C, 122(1), pp. 267-273.
[20] Wang, B., and Bocquet, M. L., 2011, "Monolayer Graphene and h-BN on Metal Substrates as Versatile Templates for Metallic Nanoclusters," Journal of Physical Chemistry Letters, 2(18), pp. 2341-2345.
[21] Katsiev, K., Losovyj, Y., Lozova, N., Wang, L., Mei, W. N., Zheng, J. X., Vescovo, E., Liu, L., Dowben, P. A., and Goodman, D. W., 2014, "The band structure of carbonmonoxide on 2-D Au islands on graphene," Applied Surface Science, 304, pp. 35-39.
[22] Zheng, J. X., Wang, L., Katsiev, K., Losovyj, Y., Vescovo, E., Goodman, D. W., Dowben, P. A., Lu, J., and Mei, W. N., 2013, "Adsorption configurations of carbon monoxide on gold monolayer supported by graphene or monolayer hexagonal boron nitride: a first-principles study," European Physical Journal B, 86(10).
[23] Hansen, L. P., Ramasse, Q. M., Kisielowski, C., Brorson, M., Johnson, E., Topsoe, H., and Helveg, S., 2011, "Atomic-scale edge structures on industrial-style MoS_2 nanocatalysts," Angewandte Chemie-International Edition, 50(43), pp. 10153-10156.
[24] Surisetty, V. R., Dalai, A. K., and Kozinski, J., 2011, "Alcohols as alternative fuels: An overview," Applied Catalysis A-General, 404(1-2), pp. 1–11.
[25] Morrill, M. R., Thao, N. T., Shou, H., Davis, R. J., Barton, D. G., Ferrari, D., Agrawal, P. K., and Jones, C. W., 2013, "Origins of Unusual Alcohol Selectivities over Mixed Mg Al Oxide-Supported K/MoS_2 Catalysts for Higher Alcohol Synthesis from Syngas," ACS Catalysis, 3(7), pp. 1665-1675.
[26] Claure, M. T., Chai, S. H., Dai, S., Unocic, K. A., Alamgir, F. M., Agrawal, P. K., and Jones, C. W., 2015, "Tuning of higher alcohol selectivity and productivity in CO hydrogenation reactions over K/MoS_2 domains supported on mesoporous activated carbon and mixed MgAl oxide," Journal of Catalysis, 324, pp. 88-97.
[27] Surisetty, V. R., Dalai, A. K., and Kozinski, J., 2010, "Synthesis of higher alcohols from synthesis gas over Co-promoted alkali-modified MoS_2 catalysts supported on MWCNTs," Applied Catalysis A-General, 385(1-2), pp. 153-162.

[28] Lv, M. M., Xie, W., Sun, S., Wu, G. M., Zheng, L. R., Chu, S. Q., Gao, C., and Bao, J., 2015, "Activated-carbon-supported K-Co-Mo catalysts for synthesis of higher alcohols from syngas," Catalysis Science & Technology, 5(5), pp. 2925-2934.
[29] Xie, W., Zhou, J. L., Ji, L. L., Sun, S., Pan, H. B., Zhu, J. F., Gao, C., and Bao, J., 2016, "Targeted design and synthesis of a highly selective Mo-based catalyst for the synthesis of higher alcohols," RSC Advances, 6(45), pp. 38741-38745.
[30] Luk, H. T., Mondelli, C., Ferre, D. C., Stewart, J. A., and Perez-Ramirez, J., 2017, "Status and prospects in higher alcohols synthesis from syngas," Chemical Society Reviews, 46(5), pp. 1358-1426.
[31] Luk, H. T., Forster, T., Mondelli, C., Siol, S., Curulla-Ferre, D., Stewart, J. A., and Perez-Ramirez, J., 2018, "Carbon nanofibres-supported KCoMo catalysts for syngas conversion into higher alcohols," Catalysis Science & Technology, 8(1), pp. 187-200.
[32] Ao, M., Pham, G. H., Sunarso, J., Tade, M. O., and Liu, S. M., 2018, "Active Centers of Catalysts for Higher Alcohol Synthesis from Syngas: A Review," ACS Catalysis, 8(8), pp. 7025-7050.
[33] Kim, J., Byun, S., Smith, A. J., Yu, J., and Huang, J. X., 2013, "Enhanced electrocatalytic properties of transition-metal dichalcogenides sheets by spontaneous gold nanoparticle decoration," Journal of Physical Chemistry Letters, 4(8), pp. 1227-1232.
[34] Osaki, T., Narita, N., Horiuchi, T., Sugiyama, T., Masuda, H., and Suzuki, K., 1997, "Kinetics of reverse water gas shift (RWGS) reaction on metal disulfide catalysts," Journal of Molecular Catalysis A: Chemical, 125(1), pp. 63-71.
[35] Besenbacher, F., Brorson, M., Clausen, B. S., Helveg, S., Hinnemann, B., Kibsgaard, J., Lauritsen, J., Moses, P. G., Norskov, J. K., and Topsoe, H., 2008, "Recent STM, DFT and HAADF-STEM studies of sulfide-based hydrotreating catalysts: Insight into mechanistic, structural and particle size effects," Catalysis Today, 130(1), pp. 86-96.
[36] Sun, D., Lu, W., Le, D., Ma, Q., Aminpour, M., Alcántara Ortigoza, M., Bobek, S., Mann, J., Wyrick, J., Rahman, T. S., and Bartels, L., 2012, "An MoS_x Structure with High Affinity for Adsorbate Interaction," Angewandte Chemie, 124(41), pp. 10430-10434.
[37] Kibsgaard, J., Chen, Z. B., Reinecke, B. N., and Jaramillo, T. F., 2012, "Engineering the surface structure of MoS2 to preferentially expose active edge sites for electrocatalysis," Nature Materials, 11(11), pp. 963-969.
[38] Ho, T. A., Bae, C., Lee, S., Kim, M., Montero-Moreno, J. M., Park, J. H., and Shin, H., 2017, "Edge-On MoS2 Thin Films by Atomic Layer Deposition for Understanding the Interplay between the Active Area and Hydrogen Evolution Reaction," Chemistry of Materials, 29(17), pp. 7604-7614.
[39] Ma, Q., Odenthal, P. M., Mann, J., Le, D., Wang, C. S., Zhu, Y. M., Chen, T. Y., Sun, D. Z., Yamaguchi, K., Tran, T., Wurch, M., McKinley, J. L., Wyrick, J., Magnone, K., Heinz, T. F., Rahman, T. S., Kawakami, R., and Bartels, L., 2013, "Controlled argon beam-induced desulfurization of monolayer molybdenum disulfide," Journal of Physics-Condensed Matter, 25(25), p. 252201.
[40] Ma, Q., Isarraraz, M., wang, C., Preciado, E., Klee, V., Bobek, S., Yamaguchi, K., li, E., Odenthal, P. M., nguyen, A., Barroso, D., Sun, D., Palacio, G. V., Gomez, M., nguyen, A., Le, D., Pawin, G., mann, J., Heinz, T. F., Rahman, T., and Bartels, L., 2014, "Postgrowth tuning of the bandgap of single-layer molybdenum disulfide films by sulfur/selenium exchange," ACS Nano, 8(5), pp. 4672-4677.

[41] Le, D., Rawal, T. B., and Rahman, T. S., 2014, "Single-Layer MoS2 with Sulfur Vacancies: Structure and Catalytic Application," Journal of Physical Chemistry C, 118(10), pp. 5346-5351.
[42] Le, D., and Rahman, T. S., 2013, "Joined edges in MoS2: metallic and half-metallic wires," Journal of Physics-Condensed Matter, 25(31).
[43] Almeida, K., Wurch, M., Geremew, A., Yamaguchi, K., Empante, T. A., Valentin, M. D., Gomez, M., Berges, A. J., Stecklein, G., Rumyantsev, S., Martinez, J., Balandin, A. A., and Bartels, L., 2018, "High-Vacuum Particulate-Free Deposition of Wafer-Scale Mono-, Bi-, and Trilayer Molybdenum Disulfide with Superior Transport Properties," ACS Appl Mater Interfaces, 10(39), pp. 33457-33463.
[44] Rawal, T. B., Le, D., and Rahman, T. S., 2017, "MoS_2–supported gold nanoparticle for CO hydrogenation," Journal of Physics: Condensed Matter, **29**(41), p. 415201.
[45] Perdew, J. P., Burke, K., and Ernzerhof, M., 1996, "Generalized gradient approximation made simple," Physical review letters, 77(18), p. 3865.
[46] Grimme, S., Antony, J., Ehrlich, S., and Krieg, H., 2010, "A consistent and accurate ab initio parametrization of density functional dispersion correction (DFT-D) for the 94 elements H-Pu," J. Chem. Phys., 132(15), pp. 154104-154122.
[47] Henkelman, G., and Jonsson, H., 2000, "Improved tangent estimate in the nudged elastic band method for finding minimum energy paths and saddle points," J. Chem. Phys., 113(22), pp. 9978-9985.
[48] Henkelman, G., Uberuaga, B. P., and Jonsson, H., 2000, "A Climbing Image Nudged Elastic Band Method for Finding Saddle Points and Minimum Energy Paths," J. Chem. Phys., 113(22), pp. 9901-9904.
[49] Lee, C., Yan, H., Brus, L. E., Heinz, T. F., Hone, J., and Ryu, S., 2010, "Anomalous Lattice Vibrations of Single- and Few-Layer MoS_2 " Acs Nano, 4(5), pp. 2695-2700.
[50] Mak, K. F., Lee, C., Hone, J., Shan, J., and Heinz, T. F., 2010, "Atomically thin MoS_2: a new direct-gap semiconductor," Physical Review Letters, 105(13), p. 136805.
[51] Splendiani, A., Sun, L., Zhang, Y. B., Li, T. S., Kim, J., Chim, C. Y., Galli, G., and Wang, F., 2010, "Emerging photoluminescence in monolayer MoS_2 " Nano Letters, 10(4), pp. 1271-1275.
[52] Rueden, C. T., Schindelin, J., Hiner, M. C., DeZonia, B. E., Walter, A. E., Arena, E. T., and Eliceiri, K. W., 2017, "ImageJ2: ImageJ for the next generation of scientific image data," BMC Bioinformatics, 18(1), p. 529.
[53] Valden, M., Lai, X., and Goodman, D. W., 1998, "Onset of catalytic activity of gold clusters on titania with the appearance of nonmetallic properties," Science, 281(5383), pp. 1647-1650.
[54] Lopez, N., Janssens, T. V. W., Clausen, B. S., Xu, Y., Mavrikakis, M., Bligaard, T., and Norskov, J. K., 2004, "On the origin of the catalytic activity of gold nanoparticles for low-temperature CO oxidation," Journal of Catalysis, 223(1), pp. 232-235.
[55] Bondzie, V. A., Parker, S. C., and Campbell, C. T., 1999, "The kinetics of CO oxidation by adsorbed oxygen on well-defined gold particles on TiO2(110)," Catalysis Letters, 63(3-4), pp. 143-151.
[56] Sahu, P., and Prasad, B. L. V., 2014, "Time and Temperature Effects on the Digestive Ripening of Gold Nanoparticles: Is There a Crossover from Digestive Ripening to Ostwald Ripening?," Langmuir, 30(34), pp. 10143-10150.

[57] Saidi, W. A., 2015, "Density Functional Theory Study of Nucleation and Growth of Pt Nanoparticles on MoS2(001) Surface," Crystal Growth & Design, 15(2), pp. 642-652.
[58] Jiang, T., Le, D., and Rahman, T. S., 2020, "MoS2-supported Au31 for CO hydrogenation: A first-principle study," Journal of Vacuum Science & Technology A, 38(3), p. 032201.
[59] Rawal, T. B., Le, D., and Rahman, T. S., 2020, "Higher alcohol synthesis from CO hydrogenation on Cu(111)-supported MoS_2," in submission.
[60] Prins, R., Egorova, M., Röthlisberger, A., Zhao, Y., Sivasankar, N., and Kukula, P., 2006, "Mechanisms of hydrodesulfurization and hydrodenitrogenation," Catalysis Today, 111(1), pp. 84-93.
[61] Kass, M. D., Janke, C. J., Connatser, R. M., and West, B., 2019, "Elastomer Swell Behavior in 1-Propanol, Diisobutylene, Cyclopentanone, and a Furan Mixture Blended in E10 and a Blendstock for Oxygenate Blending (BOB)," SAE International Journal of Fuels and Lubricants (Online), pp. Medium: ED; Size: p. 1-16.